

Accepted Manuscript

<https://doi.org/10.1016/j.jmr.2017.06.012>

Y.S. Avadhut, J. Weber, and J. Schmedt auf der Günne. Accurate determination of chemical shift tensor orientations of single-crystals by solid-state magic angle spinning NMR. *J. Magn. Reson.*, 282:89--103, 2017.

Avadhut *et al.* (2017).

Accurate determination of chemical shift tensor orientations of single-crystals by solid-state magic angle spinning NMR

Yamini S. Avadhut ^[a,c], Johannes Weber ^[b,c], Jörn Schmedt auf der Günne ^{*[b,c]}

^[a] Friedrich-Alexander-Universität Erlangen-Nürnberg

Erlangen Catalysis Resource Center

Egerlandstrasse 3, D-91058 Erlangen, Germany

^[b] Universität Siegen, Department Chemie und Biologie,

Adolf-Reichweinstraße, D-57608 Siegen, Germany

^[c] Ludwig-Maximilians-Universität München, Department Chemie,

Butenandtstraße 5-13 (D), D-81377 München, Germany

RECEIVED DATE (to be automatically inserted after your manuscript is accepted if required according to the journal that you are submitting your paper to)

E-mail: gunnej@chemie.uni-siegen.de

Abstract

An improved implementation of single-crystal magic-angle-spinning (MAS) NMR is presented which gives access to chemical shift tensors both in orientation (relative to the crystal axis system) and principal axis values. For mounting arbitrary crystals inside ordinary MAS rotors, a mounting tool is described which allows to relate the crystal orientation determined by diffraction techniques to the rotor coordinate system. The crystal is finally mounted into a MAS rotor equipped with a special insert which allows a defined reorientation of the single-crystal by 90° .

The approach is based on the idea that the dispersive spectra, which are obtained when applying read-pulses at specific rotor-phases, not only yield the size of the eigenvalues but also encode the orientation of the different chemical shift (rank-2) tensors. For this purpose two 2D-data sets with orthogonal crystal orientation are fitted simultaneously. The presented analysis for chemical shift tensors is supported by an analytical formula which allows fast calculation of phase and amplitude of individual spinning side-bands and by a protocol which solves the problem of finding the correct reference phase of the spectrum. Different rotor-synchronized pulse-sequences are introduced for the same reason. Experiments are performed on *L*-alanine and O-phosphorylethanolamine and the observed errors are analyzed in detail. The experimental data are opposed to DFT-computed chemical shift tensors which have been obtained by the extended embedded ion method.

Introduction

The chemical shift δ is a tensor of rank 2. Despite of the fact that the full tensorial property, i.e. the tensor eigenvalues (=principal axes values) and the tensor eigenvectors (=orientation of the principal axes), can give valuable information about the local molecular structure, experimental determinations of the full tensor information are comparably scarce. Most solid-state NMR investigations are restricted to the principal axes values.¹ The reasons why eigenvectors have been reported seldomly are (i) necessary commercial goniometer probes are not widely available, (ii) homonuclear dipole-dipole couplings may limit resolution, and (iii) low sensitivity.

Examples of such full investigations are given for various nuclei and with different NMR experiments, for example ¹³C (see refs 2–6), ¹⁴N (ref. 7), ¹⁹F (ref. 8), ³¹P (refs. 9–12), ⁵⁹Co (ref. 13), and ²⁰⁷Pb (ref. 14) some of which have gained tremendous importance because the results serve as reference values in NMR methodology development^{15–19} and in applications for determining bond and dihedral angles.^{12,20–23} These experiments are commonly performed with the help of static measurements in goniometer NMR probes.^{3,19} The possibility to obtain single crystal MAS spectra from powders²⁴ by selective excitation of a powder subset is a very interesting option but does not yield absolute tensor orientations.

An alternative was introduced by Kunath-Fandrei *et al.*²⁵ who suggested using magic-angle-spinning (MAS) NMR where the rotor phase at the beginning of the read-pulse is systematically varied. At moderate spinning frequencies the observed spectra contain a sideband pattern where the dispersive line shapes of the individual spinning sidebands encode the chemical shift tensor orientation. The authors showed that the sideband pattern contains enough information to determine shift tensor eigenvectors from two different two-dimensional (2D) data sets. In their study they made use of a single-crystal of high symmetry and a simple morphology which eased the data analysis. Klymachyov and Dalal²⁶ have used single crystal MAS NMR for the characterization of phase transitions. Kentgens *et al.*^{27,28} showed that single-crystal MAS NMR has sufficient sensitivity if combined with microcoils to get tensor information even in case of minute crystals. Similar experiments have also been performed for oriented polymers³⁰. Earlier it had already been shown MAS spectra of single-crystals become absorptive, when the rotor-phase at the read-pulse is averaged over a full revolution of the

Avadhut *et al.* (2017).

rotor ("carousel" averaging)³¹, which will become useful to determine the reference phase for the data analysis.

In this work we extend the work by Kunath-Fandrei *et al.* in theory and hardware to allow a routine application of this technique. To this end several issues had to be addressed: a practical way for mounting arbitrary single-crystals in a defined way (section hardware), efficient data analysis by an analytical formula for the line shape function (section theory) as well as an analytical protocol including special pulse sequences which help to stabilize the baseline and define reference phase (section pulse sequences and protocol).

During the rather long time between essentially finishing the current work (April 2011) and writing down the current manuscript, several papers appeared, which deal with the derivation of the dispersive side band pattern for a single crystal making use of irreducible spherical tensor representations for the chemical shift (anisotropy) and Wigner matrices.^{32,33,34} Earlier the same strategy was used for the derivation of the tensor of quadrupolar interaction²⁷, and in fact was already introduced for arbitrary interactions in a review by Antzutkin³⁵ as well as the famous paper on rotating solids by Maricq and Waugh³⁶. Therefore, we omit this derivation, but instead provide a description in Cartesian space in complete analogy to Herzfeld and Berger.³⁷

Theory

Coordinate systems and transformations

For the determination of tensor orientations from single-crystal MAS experiments it is convenient to introduce seven right-handed, Cartesian coordinate systems denoted as $\{P, C, G, D, W, R, L\}$ (=frames) as shown in Figure 1. Well established in NMR under MAS conditions are the principal axis frame of a specific interaction (P), the crystal (alternatively molecular) frame (C), the MAS rotor frame (R) and the laboratory frame (L) in which the observation of the free induction decay (FID) is made. For single-crystal MAS NMR we need three extra frames, because the orientation of the crystal is determined with diffraction experiments prior to the NMR experiments on a diffractometer (frame D) while the crystal orientation is approximately conserved by mounting it onto a goniometer adapter (G) before being glued into a small cube (German: Würfel, W) whose orientation relative to R must be determined in order to relate the crystal frame C to the rotor frame R . The precise definitions of the individual frames are given as follows:

1. P is the principal axes frame. It consists of the three orthonormal eigenvectors $\{\mathbf{e}_1^P, \mathbf{e}_2^P, \mathbf{e}_3^P\}$ of the chemical shift tensor.
2. C is the crystal axes frame, whose basis vectors \mathbf{e}_i^C are defined via an orthogonalization procedure from the (real-space) crystal axes \mathbf{a} , \mathbf{b} , and \mathbf{c} : $\mathbf{e}_1^C = \mathbf{a}/|\mathbf{a}|$, $\mathbf{e}_2^C = (\mathbf{b} - \mathbf{b} \cdot \mathbf{e}_1^C) / |(\mathbf{b} - \mathbf{b} \cdot \mathbf{e}_1^C)|$, $\mathbf{e}_3^C = \mathbf{e}_1^C \times \mathbf{e}_2^C$. In case of a cubic or orthorhombic crystal the expressions simplify to $\mathbf{e}_1^C = \mathbf{a}/|\mathbf{a}|$, $\mathbf{e}_2^C = \mathbf{b}/|\mathbf{b}|$, $\mathbf{e}_3^C = \mathbf{c}/|\mathbf{c}|$. In case of a monoclinic crystal the axes are $\mathbf{e}_1^C = \mathbf{a}/|\mathbf{a}|$, $\mathbf{e}_2^C = \mathbf{b}/|\mathbf{b}|$, $\mathbf{e}_3^C = \mathbf{e}_1^C \times \mathbf{e}_2^C = \mathbf{c}^*/|\mathbf{c}^*|$, where \mathbf{c}^* is the third basis vector of the reciprocal cell.
3. G is the goniometer adapter frame. The origin of its basis vectors \mathbf{e}_i^G is located at the intersection point of the rotation axis and the fixation plane. \mathbf{e}_1^G points away from the notch in the base ring of the adaptor, \mathbf{e}_2^G is along the rotation axis (and perpendicular to the fixation plane) of the adaptor pointing towards its tip, and $\mathbf{e}_3^G = \mathbf{e}_1^G \times \mathbf{e}_2^G$.
4. W is the frame of the cube (german: "Würfel"), that hosts the single-crystal and is inserted to the MAS rotor. Three cube faces were marked with different hatching (vertical-red-lines, horizontal-green-lines, cross-blue-lines) and assigned as the normal planes of \mathbf{e}_i^W , $i=1,2,3$, respectively. The face marked with cross-lines contains the borehole, i.e. \mathbf{e}_3^W is parallel with the long axis of the cylindrical borehole. \mathbf{e}_1^W and \mathbf{e}_2^W are chosen along the intersecting edges of horizontal-green-cross and vertical-red-cross line faces, respectively. *Parallel* placement of cube W in the rotor is defined as \mathbf{e}_1^W being parallel to the rotor axis \mathbf{e}_1^R (defined below) with $\mathbf{e}_1^W \cdot \mathbf{e}_1^R = 1$, $\mathbf{e}_2^W \cdot \mathbf{e}_2^R = 1$, and $\mathbf{e}_3^W \cdot \mathbf{e}_3^R = 1$; *perpendicular* placement means that $\mathbf{e}_1^W \cdot \mathbf{e}_3^R = 1$, $\mathbf{e}_2^W \cdot \mathbf{e}_2^R = 1$, and $\mathbf{e}_3^W \cdot \mathbf{e}_1^R = -1$ via rotating the cube by 90° around \mathbf{e}_2^W .
5. D is the diffractometer frame. It is close (but not identical) to G with its basis vectors defined as: $\mathbf{e}_1^D = \mathbf{e}_2^D \times \mathbf{e}_3^D$ is perpendicular to the rotation axis of the goniometer and the X-ray beam (pointing away from the CCD camera in the parking position on our diffractometer), \mathbf{e}_2^D is along the rotation axis (and identical to \mathbf{e}_2^G) and \mathbf{e}_3^D is pointing towards X-ray beam source. In our case, we found that D differs from G via clockwise rotation by 0.56° around \mathbf{e}_2^G . The

diffractometer frame may vary for different diffractometers.

6. R is the (MAS) rotor axis system, and defined by: \mathbf{e}_3^R is the rotor spinning axis, \mathbf{e}_1^R is along the line from the center towards a point on the rotor wall at which the anticlockwise rotation is optically detected using white-to-black contrast, and $\mathbf{e}_2^R = \mathbf{e}_3^R \times \mathbf{e}_1^R$.
7. L is the Lab coordinate system. It is defined by: \mathbf{e}_3^L is along the external magnetic field \mathbf{B}_0 , \mathbf{e}_1^L is perpendicular to \mathbf{e}_3^L and lies in the plane spanned by the symmetry axis of the solenoid coil and \mathbf{B}_0 , and $\mathbf{e}_2^L = \mathbf{e}_3^L \times \mathbf{e}_1^L$.

The relative orientations between any two frames can be expressed by direction cosines or alternatively by Euler angles.³⁸ A general rotation matrix \mathbf{R} to transform a vector or a tensor from one coordinate system (A) to another (B) can be decomposed as the product of the three individual rotations

$$\mathbf{R}(\Omega_{AB}) = \mathbf{R}(\alpha_{AB}, \beta_{AB}, \gamma_{AB}) = \mathbf{R}_z(\alpha) \mathbf{R}_{y'}(\beta) \mathbf{R}_{z''}(\gamma) \quad , \quad (1)$$

where Ω_{AB} is the symbol denoting a set of Euler angles $(\alpha_{AB}, \beta_{AB}, \gamma_{AB})$ and $\mathbf{R}_z(\alpha)$, $\mathbf{R}_{y'}(\beta)$, $\mathbf{R}_{z''}(\gamma)$ are rotation matrices in Cartesian space which describe a rotation around z -axis by an angle α , rotation around the newly formed y' -axis by an angle β and a last rotation around the newly formed z'' -axis through γ , respectively.³⁸ Here, the $\{x, y, z\}$ indicates the starting reference frame axes while primes on the axes denote the intermediate rotated frames. The $\mathbf{R}(\Omega_{AB})$ rotation matrix with the set of Euler angles $(\alpha_{AB}, \beta_{AB}, \gamma_{AB})$ is defined as,

$$\mathbf{R}(\Omega_{AB}) = \begin{pmatrix} \cos \gamma_{AB} & \sin \gamma_{AB} & 0 \\ -\sin \gamma_{AB} & \cos \gamma_{AB} & 0 \\ 0 & 0 & 1 \end{pmatrix} \cdot \begin{pmatrix} \cos \beta_{AB} & 0 & -\sin \beta_{AB} \\ 0 & 1 & 0 \\ \sin \beta_{AB} & 0 & \cos \beta_{AB} \end{pmatrix} \cdot \begin{pmatrix} \cos \alpha_{AB} & \sin \alpha_{AB} & 0 \\ -\sin \alpha_{AB} & \cos \alpha_{AB} & 0 \\ 0 & 0 & 1 \end{pmatrix} \quad , \quad (2)$$

We followed the Rose convention³⁸ and passive rotations as described by Schmidt-Rohr and Spiess³⁹ for the definitions of Euler angles and rotation matrices.

Analytic treatment of single-crystal MAS NMR signals

In Fourier-transform NMR, the spectrum $S(\omega)$ of a single nucleus n can be described by⁴⁰

$$S(\omega) = aL(\omega; \omega_n^L, \lambda_n) \exp\{i(\theta + \theta_0)\} \quad , \quad (3)$$

where $S(\omega) \in \mathbb{C}$ is a complex valued function depending on the frequency ω , the signal amplitude a , the Larmor frequency of the nucleus ω_n^L , the peak-width parameter λ_n , the signal phase θ , and the phase correction angle of zeroth order θ_0 used in post processing of the NMR spectrum. The complex Lorentzian, L , is defined as

$$L(\omega; \omega_n^L, \lambda_n) = \underbrace{\frac{\lambda_n}{\lambda_n^2 + (\omega - \omega_n^L)^2}}_A + i \underbrace{\frac{-(\omega - \omega_n^L)}{\lambda_n^2 + (\omega - \omega_n^L)^2}}_D \quad , \quad (4)$$

A is called the absorption Lorentzian, D the dispersion Lorentzian. Both θ and θ_0 do not depend on ω . θ_0 is adjusted during the post processing ("phasing") of the NMR spectrum, so that $\theta + \theta_0 = 0$, which causes the real part of a carousel averaged 1-crystal NMR spectrum to have a purely absorptive line shape

$$\text{Re}[S(\omega)] = aA(\omega; \omega_n^L, \lambda_n) \quad , \quad (5)$$

At present, solid-state NMR spectra of crystalline compounds are mostly recorded for powdered samples, which forms a perfect carousel average and hence can be phased to purely absorptive line shapes. If the nucleus under investigation is bound in a low-symmetric environment, the chemical shift anisotropy (CSA) leads to a signal broadening, which reflects the dependency of the resonance signal on the different orientations of the crystallites (or more accurately: the chemical shift tensor) with respect to the magnetic field. Under MAS conditions at moderate spinning frequencies ($\nu_{rot} < \delta_{aniso} \nu_{ref}$) the CSA is partly averaged out, so that the resonance signal splits into a central band and various spinning sidebands (SSBs), all of which have the same signal phase θ . Thus, the spectrum remains purely absorptive. In the following we will drop the subscript n which refers to nuclei from different chemical environments.

Contrarily, in rotor-synchronized MAS NMR spectra of single crystalline (non-powdered) samples the phases of the SSBs generally differ from one another so that no phasing to a purely absorptive spectrum is possible. Instead, the line shape of each SSB is a mixture of absorptive and dispersive parts

Avadhut *et al.* (2017).

depending on the tensor orientation in the magnetic field.^{36,41} By rotor-synchronization we understand in this context, that the radio frequency (rf) excitation pulse is fixed with respect the rotor position. If the rf excitation is evenly distributed over the rotor phase, e.g. by numerous excitations at random times, the single-crystal MAS spectra show purely absorptive line shapes similar to powdered sample.^{41,42} The complex NMR signal $S(t)$, which is obtained by⁴³,

$$S(t) \sim \text{tr} \{ \rho(t) \hat{I}^+ \} , \quad (6)$$

where $\hat{I}^+ = \hat{I}_x + i \hat{I}_y$ is a shift operator. For the time-dependent Hamiltonian, using Baker-Hausdorff relation for time evolution series³⁹, the density matrix is proportional to,

$$\rho(t) = \exp \int_0^t i \omega^L dt = \exp i \left\{ -\gamma_{nuc} B_0 \int_0^t \delta_{zz}^L dt \right\} , \quad (7)$$

In this work, we follow the classical approach of Herzfeld *et al.*,³⁷ but extend it to the calculation of the intensities and the phases of dispersive spinning sidebands. Figure 2 shows the chosen laboratory coordinate system. Under MAS conditions the sample is spun at an angular frequency ω_r around the rotor axis \mathbf{e}_3^R which has an angle β_{RL} relative to the applied magnetic field \mathbf{B}_0 . The field lines of the latter lie along \mathbf{e}_3^L . Hence, in the R -frame the sample sees the direction of the static magnetic field oscillating according to the following equation (see also Figure 2)

$$\left(\mathbf{e}_3^L \right)^R = \left(\sin \beta_{RL} \cos \alpha_{RL}, \sin \beta_{RL} \sin \alpha_{RL}, \cos \beta_{RL} \right) , \quad (8)$$

where

$$\alpha_{RL} = \alpha_0^{RL} + \omega_r t , \quad (9)$$

is the rotation angle of the rotor measured at time t relative to an offset α_0^{RL} .

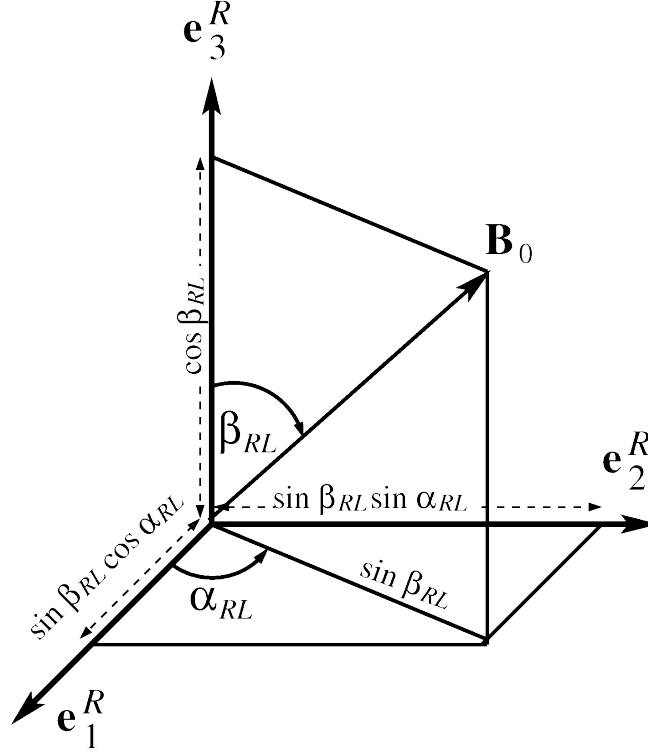


Figure 2: The coordinate system with the rotor axis frame as reference; the (0,0,1) vector is the axis of rotation of the sample; \mathbf{B}_0 is a unit vector in the direction of the applied magnetic field.³⁷

The precession frequency of a given spin is

$$\omega^L = -\gamma_{nuc} B_0 (\mathbf{B}_0 \cdot \delta^R \cdot \mathbf{B}_0^T) , \quad (10)$$

where δ^R is the chemical shift tensor for that spin in a molecule/crystal expressed in the rotor axis frame. δ^R may be obtained from δ^C , which is the shift tensor expressed in the orthogonalized crystal coordinate system, according to

$$\delta^R = \mathbf{R}(\Omega_{CR}) \left(\mathbf{R}(\Omega_{PC}) \cdot \delta^P \cdot \mathbf{R}^{-1}(\Omega_{PC}) \right) \mathbf{R}^{-1}(\Omega_{CR}) , \quad (11)$$

where δ^P is the chemical shift tensor in the principal axis frame (P) in which the chemical shift tensor is diagonal.

$$\delta^P = \begin{pmatrix} \delta_{xx}^P & 0 & 0 \\ 0 & \delta_{yy}^P & 0 \\ 0 & 0 & \delta_{zz}^P \end{pmatrix} . \quad (12)$$

In the secular approximation only the z -component of δ^L is of interest in the laboratory frame (L), whose relation to δ_{iso} and the components δ_{ii}^R is obtained by combination of equation (10) and (11):

$$\delta_{zz}^L = \left[\delta_{iso} + \frac{1}{2} (3 \cos^2 \beta_{RL} - 1) (\delta_{zz}^R - \delta_{iso}) \right] + \sin^2 \beta_{RL} \left[\frac{1}{2} (\delta_{xx}^R - \delta_{yy}^R) \cos(2 \alpha_{RL}) + \delta_{xy}^R \sin(2 \alpha_{RL}) \right] + 2 \sin \beta_{RL} \cos \beta_{RL} \left[\delta_{xz}^R \cos \alpha_{RL} + \delta_{yz}^R \sin \alpha_{RL} \right] \quad (13)$$

Evaluation of ω^L , combining equations (7) and (13) and, shows that it contains a time independent term, a term which oscillates through α_{RL} at $2 \omega_r$, and a term which oscillates at ω_r ,

$$\omega^L = (-\gamma_{nuc} B_0) \left(\delta_{iso} + \frac{1}{2} (3 \cos^2 \beta_{RL} - 1) (\delta_{zz}^R - \delta_{iso}) + \sin^2 \beta_{RL} \left[\frac{1}{2} (\delta_{xx}^R - \delta_{yy}^R) \cos(2 \alpha_{RL}) + \delta_{xy}^R \sin(2 \alpha_{RL}) \right] + 2 \sin \beta_{RL} \cos \beta_{RL} (\delta_{xz}^R \cos \alpha_{RL} + \delta_{yz}^R \sin \alpha_{RL}) \right) \quad (14)$$

For the magic angle $\beta_{RL} = \beta_{magic} = \arccos(1/\sqrt{3})$, the term $(3 \cos^2 \beta_{RL} - 1)$ in equation (14) becomes zero, and hence

$$\omega^L = (-\gamma_{nuc} B_0) \left(\delta_{iso} + \frac{2}{3} \left(\frac{\delta_{xx}^R}{2} \cos(2 \alpha_{RL}) - \frac{\delta_{yy}^R}{2} \cos(2 \alpha_{RL}) + \delta_{xy}^R \sin(2 \alpha_{RL}) \right) + \frac{2\sqrt{2}}{3} (\delta_{xz}^R \cos \alpha_{RL} + \delta_{yz}^R \sin \alpha_{RL}) \right) \quad (15)$$

The free induction decay for the entire sample is given by equation (7)

Avadhut *et al.* (2017).

$$\begin{aligned}
\rho(t) = \exp\{i\theta(\alpha_{PL}, \beta_{PL}, \gamma_{PL}, t)\} &= \exp\left\{i(-\gamma_{nuc} B_0)\left(\delta_{iso} t\right) + \left(\frac{1}{2\omega_r}\right)\left(\frac{2}{3}\right)\left[\frac{\delta_{xx}^R}{2} \sin 2\alpha_{RL} - \frac{\delta_{xx}^R}{2} \sin 2\alpha_0^{RL}\right]\right. \\
&\quad - \left(\frac{1}{2\omega_r}\right)\left(\frac{2}{3}\right)\left[\frac{\delta_{yy}^R}{2} \sin 2\alpha_{RL} + \frac{\delta_{yy}^R}{2} \sin 2\alpha_0^{RL}\right] + \\
&\quad \left.\left(\frac{1}{2\omega_r}\right)\left(\frac{2}{3}\right)\left[\delta_{xy}^R \sin\left(2\alpha_{RL} - \frac{\pi}{2}\right) - \delta_{xy}^R \sin\left(2\alpha_0^{RL} - \frac{\pi}{2}\right)\right]\right. \\
&\quad + \left(\frac{1}{\omega_r}\right)\left(\frac{2\sqrt{2}}{3}\right)\left[\delta_{xz}^R \sin \alpha_{RL} - \delta_{xz}^R \sin \alpha_0^{RL}\right] + \\
&\quad \left.\left(\frac{1}{\omega_r}\right)\left(\frac{2\sqrt{2}}{3}\right)\left[\delta_{yz}^R \sin\left(\alpha_{RL} - \frac{\pi}{2}\right) - \delta_{yz}^R \sin\left(\alpha_0^{RL} - \frac{\pi}{2}\right)\right]\right\} \quad (16)
\end{aligned}$$

The NMR signal generated by any pulse sequence can be expressed as,⁴⁰

$$S(t) = \sum_N a_N \exp\{i(\omega_N t + \theta_N)\} \exp\{-t/T_2\} \quad , \quad (17)$$

where, a_N is the N^{th} sideband intensity, ω_N is the N^{th} sideband resonance frequency, θ_N is the N^{th} sideband phase of the signal component, and $1/T_2$ is a damping rate constant. Hereafter $1/T_2$ is neglected for simplicity of an analytical function. Equation (16) can be expressed in the form of equation (17) using the following property of the Bessel functions of the first kind⁴⁴⁻⁴⁶

$$\exp\{i z \sin \theta\} = \sum_{n=-\infty}^{\infty} J_n(z) \exp\{i n \theta\} \quad . \quad (18)$$

It follows that

$$\begin{aligned}
&\exp\left\{i\left[\theta_0 + C_1 \sin \theta_1 + C_2 \sin \theta_2 + \dots + C_n \sin \theta_n\right]\right\} = \\
&\sum_{n_1=-\infty}^{\infty} \sum_{n_2=-\infty}^{\infty} \dots \sum_{n_n=-\infty}^{\infty} J_{n_1}(C_1) J_{n_2}(C_2) \dots J_{n_n}(C_n) \times \exp\left\{i\left[\theta_0 + n_1 \theta_1 + n_2 \theta_2 + \dots + n_n \theta_n\right]\right\} \quad . \quad (19)
\end{aligned}$$

Thus, equation (16) becomes,

Avadhut *et al.* (2017).

$$\begin{aligned}
\rho(t) = \exp\left[i\theta(\alpha_{PL}, \beta_{PL}, \gamma_{PL}, t)\right] &= \sum_{j=-\infty}^{\infty} J_j(\kappa_{xx}^R) \sum_{j'=-\infty}^{\infty} J_{j'}(\kappa_{xx}^R) \sum_{k=-\infty}^{\infty} J_k(\kappa_{yy}^R) \sum_{k'=-\infty}^{\infty} J_{k'}(\kappa_{yy}^R) \\
&\sum_{l=-\infty}^{\infty} J_l(\kappa_{xy}^R) \sum_{l'=-\infty}^{\infty} J_{l'}(\kappa_{xy}^R) \sum_{m=-\infty}^{\infty} J_m(\kappa_{xz}^R) \\
&\sum_{m'=-\infty}^{\infty} J_{m'}(\kappa_{xz}^R) \sum_{n=-\infty}^{\infty} J_n(\kappa_{yz}^R) \sum_{n'=-\infty}^{\infty} J_{n'}(\kappa_{yz}^R) \times \\
&\exp\left\{i\left(-\gamma_{nuc} B_0 \delta_{iso} t + \omega_r t (2j - 2k + 2l + m + n) + \right. \right. \\
&\alpha_0^{RL} [2(j - j') - 2(k - k') + 2(l - l') + (m - m') + (n - n')] \\
&\left. \left. - \frac{\pi}{2} [(l - l') + (n - n')] \right)\right\}
\end{aligned} \tag{20}$$

where,

$$\begin{aligned}
\kappa_{xx}^R &= -\gamma_{nuc} B_0 \left(\frac{1}{2\omega_r}\right) \left(\frac{\delta_{xx}^R}{3}\right) \quad \wedge \quad \kappa_{yy}^R = -\gamma_{nuc} B_0 \left(\frac{1}{2\omega_r}\right) \left(\frac{\delta_{yy}^R}{3}\right) , \\
\kappa_{xy}^R &= -\gamma_{nuc} B_0 \left(\frac{1}{2\omega_r}\right) \left(\frac{2}{3}\right) \delta_{xy}^R , \\
\kappa_{xz}^R &= -\gamma_{nuc} B_0 \left(\frac{1}{\omega_r}\right) \left(\frac{2\sqrt{2}}{3}\right) \delta_{xz}^R \quad \wedge \quad \kappa_{yz}^R = -\gamma_{nuc} B_0 \left(\frac{1}{\omega_r}\right) \left(\frac{2\sqrt{2}}{3}\right) \delta_{yz}^R .
\end{aligned} \tag{21}$$

The free induction decay in equation (20) consists of a central resonance at the isotropic chemical shift and a series of non-absorptive spinning sidebands spaced ω_r apart.

The intensities and the phases of the sidebands

As per Herzfeld *et al.*,³⁷ it is convenient to call the sideband located at $N\omega_r$ from the isotropic resonance the N^{th} sideband. If the position of the isotropic resonance is not known, the N^{th} sideband may be identified as the line which moves $N(\Delta\omega_r)$ when the spinning speed is changed by $\Delta\omega_r$. Using $N = 2j - 2k + 2l + m + n$ as substitution in equation (20), the relative intensity and the phase of the N^{th} sideband is

Avadhut *et al.* (2017).

$$\begin{aligned}
S_N = & \sum_{j=-\infty}^{\infty} J_j(\kappa_{xx}^R) \sum_{j'=-\infty}^{\infty} J_{j'}(\kappa_{xx}^R) \sum_{k=-\infty}^{\infty} J_k(\kappa_{yy}^R) \sum_{k'=-\infty}^{\infty} J_{k'}(\kappa_{yy}^R) \sum_{l=-\infty}^{\infty} J_l(\kappa_{xy}^R) \\
& \sum_{l'=-\infty}^{\infty} J_{l'}(\kappa_{xy}^R) \sum_{m'=-\infty}^{\infty} J_{m'}(\kappa_{xz}^R) \sum_{n=-\infty}^{\infty} J_n(\kappa_{yz}^R) \sum_{n'=-\infty}^{\infty} J_{n'}(\kappa_{yz}^R) J_{N-2j+2k-2l-n}(\kappa_{xz}^R) \\
& \times \exp \left\{ i \left(\alpha_0^{RL} [2(j-j') - 2(k-k') + 2(l-l') \right. \right. \\
& \left. \left. + (N-2j+2k-2l-n-m') + (n-n') \right] \right. \\
& \left. - \frac{\pi}{2} [(l-l') + (n-n')] \right\} \quad (22)
\end{aligned}$$

The infinite sums and Bessel's function in equation (22) may be eliminated by using following property⁴⁴⁻⁴⁶,

$$J_n(z) = \frac{1}{2\pi} \int_0^{2\pi} \exp[iz \sin \theta - in\theta] d\theta \quad (23)$$

and equation (18).

The resultant equation can be written as

$$\begin{aligned}
S_N = & \exp \left\{ i \left(-\kappa_{xx}^R \sin(2\alpha_0^{RL}) + \kappa_{yy}^R \sin(2\alpha_0^{RL}) \right. \right. \\
& \left. \left. + \kappa_{xy}^R \cos(2\alpha_0^{RL}) - \kappa_{xz}^R \sin(\alpha_0^{RL}) + \kappa_{yz}^R \cos(\alpha_0^{RL}) \right) \right\} \\
& \times \frac{1}{2\pi} \int_0^{2\pi} \exp \left\{ i(\alpha_0^{RL} - \theta)N + \kappa_{xx}^R \sin(2\theta) - \kappa_{yy}^R \sin(2\theta) - \kappa_{xy}^R \cos(2\theta) \right. \\
& \left. + \kappa_{xz}^R \sin(\theta) - \kappa_{yz}^R \cos(\theta) \right\} d\theta \quad (24)
\end{aligned}$$

Equation (24) is an analytical function to calculate the intensities and the phases of the dispersive spinning sidebands, encoded in the complex valued S_N .

Symmetry related shielding tensors in single-crystals

It has been recognized early that two crystallographically equivalent nuclei (CEN), i.e. a pair of nuclei which belongs to the same crystallographic site (alias two representatives of a crystallographic orbit in IUCR terminology⁴⁷), do not necessarily have the same shielding tensor contribution for a given orientation in a single crystal NMR experiment.⁴⁸ Although these nuclei and their electronic environments are related to one another by some symmetry operation, the orientation of their

corresponding nuclear magnetic shielding tensors relative to the magnetic field vectors can be different. This becomes manifest in single crystal NMR rotation plots where some of the CEN show different chemical shifts depending on the crystal orientation, while others don't. For example, four different NMR signals are visible from the eight crystallographically equivalent ^{31}P nuclei the unit cell of 2-aminoethyl-phosphonic acid.⁹ Single-crystal MAS-NMR spectra which are in the focus of the present work are affected by this inequivalence as well. In order to decide whether two CEN have the same shielding tensor contribution to the Hamiltonian or not, it is helpful to investigate the symmetry relationships between them, which are given for all possible space groups in the *International Tables Of Crystallography Volume A*.⁴⁷ Two CEN will in general have the same contribution if their tensors have the same orientation, we thus call them "orientationally equivalent" to distinguish this case from the terms "chemical equivalence" and "magnetic equivalence" which have been defined in different ways depending on context.^{40,49}

The question whether two representatives are orientationally equivalent can be answered by investigation of the symmetry elements of the space group: A pair of CEN related by a translation or an inversion will be orientationally equivalent, since the (symmetric part of the) chemical shift tensor is invariant to these symmetry operations. However, other symmetry operations like reflections, rotations and rotoinversions by angles different from 360° lead to orientational inequivalence. To find out orientational (in)equivalences quickly, and to derive the orientations of shielding tensors of nuclei from the same crystallographic orbit, we follow the general approach described in chapter 11.1 of ref.⁴⁷ and set up a transformation matrix $\mathbf{W}^{(k)}$ and a translation vector $\mathbf{w}^{(k)}$. The vector $\mathbf{w}^{(k)}$ can be omitted for the reason mentioned above. Although these matrices define transformations in fractional coordinate space, their principal character stays the same when transformed to orthogonalized Cartesian coordinates. The latter transformation is needed to calculate the reorientation of the shielding tensor of a magnetically inequivalent site.

In SIMPSON^{50,51} simulations of the single-crystal NMR spectra care must be taken for orientationally inequivalent nuclei and a simulation for each of them has to be done. In order to save computational resources, the individual orientations can be simulated as separate spin systems. A different strategy was used by Hansen *et al.*⁵² The observed spectrum is a superposition of the orientationally inequivalent nuclei, with the relative abundance of the respective orientations as weights.

Phase correction for single-crystal MAS NMR / Phase reference in single-crystal MAS NMR

In general, single-crystal NMR spectra under MAS are dispersive in nature. The line shape of each spinning sideband of single-crystal spectra has a particular phase which is given by equation (24)^{36,41}. In single-crystal MAS NMR, the signal phase is important as it provides information about chemical shift tensor orientation. In order to obtain a stable phase reference we use the fact that a single-crystal MAS NMR spectrum averaged over an infinite number of evenly spaced starting angles α_{PR} generates an absorptive spectrum, which has been termed carousel averaging.³¹

An interesting question is how many uniformly spaced starting angles α_{PR} will be necessary to get an sufficiently absorptive spectrum for phase referencing in single-crystal MAS NMR. Figure 3 shows the signal averaging for various numbers N_c of seats in carousel. It is observed that the absorptive character of the spectrum rapidly improves for increasing an increasing number of seats N_c . For example, the absorptive character for a spectrum with $N_c=20$ (Figure 3), shows a signal phases below 0.05° for the four sidebands of highest intensity. The number N_c necessary to achieve a close-to-absorptive spectrum may however depend on the chemical shift tensor.

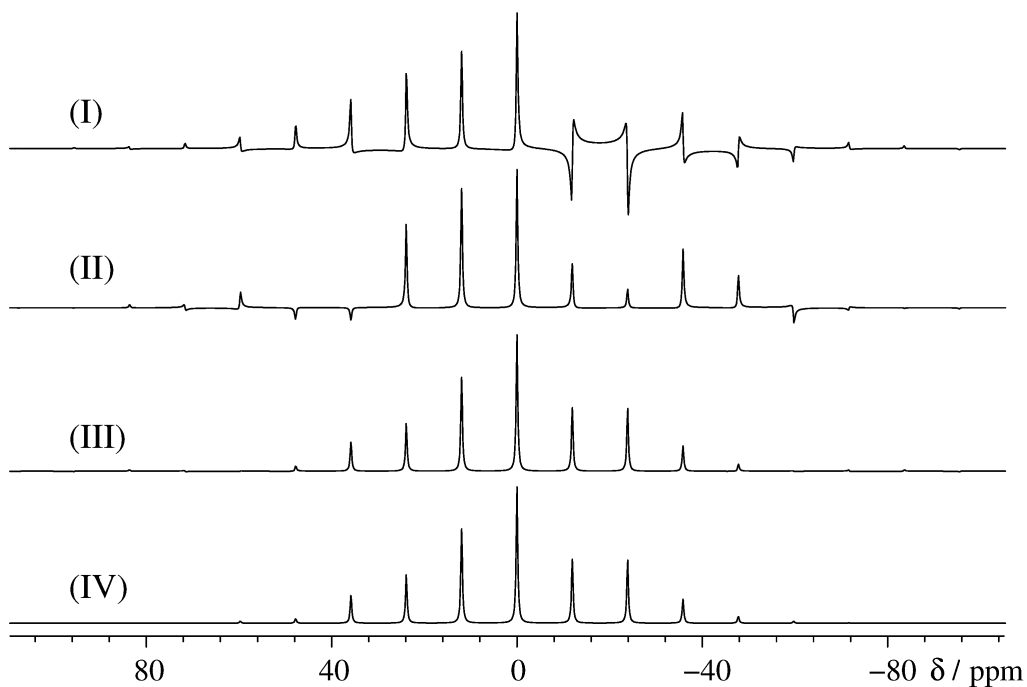


Figure 3: Signal averaging of single-crystal magic angle spinning spectra for (I) $N_c=2$, (II) $N_c=5$, (III) $N_c=10$, and (IV) $N_c=20$ being the number of “seats”, i.e. starting angles α_{RL} in the carousel average; a sufficiently absorptive spectrum is observed for $N_c=20$ (IV); numerical simulation parameters are: $\omega_r/2\pi=1.5\text{kHz}$, chemical shift anisotropy parameter $\delta_{aniso}=-68.3\text{ppm}$, and asymmetry parameter $\eta=0.76$; single-crystal orientation specified by Euler angles $\alpha_{PR}=350^\circ$, $\beta_{PR}=95^\circ$, and $\gamma_{PR}=100^\circ$.

Experimental Details

Hardware

Single-crystal MAS NMR in principle can be done without any specialized hardware. However, if the aim of the investigation is the determination of the chemical shift tensor orientation in the (orthogonalized) crystal axes system, the crystal has to be either of a simple morphology²⁵ or its orientation, i.e., the orientation of the crystallographic unit cell in the laboratory frame, has to be determined independently. A convenient way to determine it is offered by standard diffraction techniques. In the following we describe two home-made tools which represent a minor financial investment comparable to a few ceramic rotors, which allowed us to use a standard MAS probe for single-crystal MAS NMR experiments. The basic idea is to transfer the information about the crystal orientation from the goniometer of the diffractometer into a MAS rotor insert, by gluing the crystal into a small cube which can then be put into a cubic void of an insert which fits the cylindric void of a MAS rotor as described in Figure 4.

Single-crystal mounting equipment

In Figure 4-I a tool is shown which can be used for mounting a single-crystal with a dimension of about 1 mm³ in a magic angle spinning (MAS) rotor. This equipment comprises the following parts. A standard goniometer is used to measure a single-crystal orientation on an X-ray diffractometer. The goniometer adapter (**c**) with known orientation of the single-crystal can be screwed on the goniometer holder (**b**) that is fixed permanently to plate (**a**). The cube (**e**) with 2 mm³ dimension is tightened to a movable cube holder (**f**). The cube is made from polychlorotrifluoroethylene (PCTFE or Kel-F). Single-crystal is transferred with a linear bearing into the opening of a cube with a cylindrical void with known orientation. The single-crystal can be glued into the cube using suitable glue for example 2-components epoxy resine.

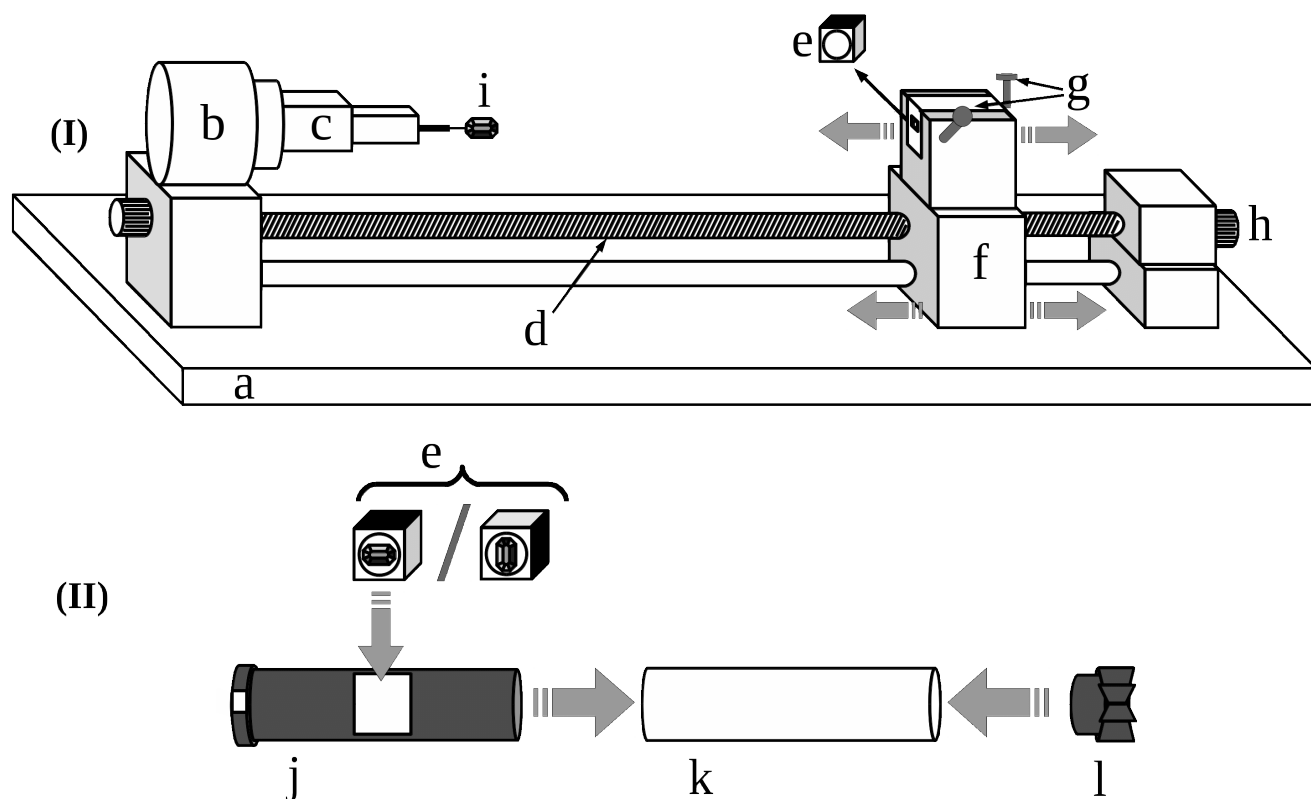


Figure 4: A complete hardware assembly for a rotorsynchronized magic angle spinning NMR experiment of a single-crystal; a base plate **a** ; a goniometer holder **b** ; a goniometer adapter **c** with the single-crystal **i** a rod **d** ; a cube **e** ; a movable cube holder **f** ; tightening screws **g** ; an adjustment wheel **h** ; a black polyoxymethylene rotor insert with a cavity for the cube **e** and a white mark inserted in bottom cap as a single piece **j** ; and a 4 mm both open end MAS rotor **k** with a drive cap **l** .

Rotor insert

To determine the orientation of the single-crystal in the MAS rotor, it is necessary to achieve the light detection mark which has a fixed position on the rotor. This can be achieved using a specially designed rotor with three parts, a rotor insert with a bottom cap as a single piece (**j**) which can be inserted/fixe in a both open ended 4 mm ZrO_2 MAS rotor (**k**) with a drive cap (**l**) on the top as shown in Figure 4-II. The rotor insert is made of black polyoxymethylene (POM) material. A small middle strip of the bottom cap of the insert is replaced by white polyvinyl chloride (PVC) to achieve the fixed light

detection mark on the MAS rotor for spin detection. At the center of the insert, a cubic hole is pressed with the exact dimensions of the sample cube, so that the single-crystal is located in the homogeneous part of the rf coil. Finally, the complete rotor insert including the sample cube as a single unit is placed in a both open ended 4 mm ZrO₂ MAS rotor (**k**) with a drive cap (**I**) (Figure 4-II).

The cube assembly gives freedom to choose two different orientations for a rotorsynchronized MAS NMR of a single-crystal, which is sufficient to allow a high-accuracy determination of the chemical shift tensor orientations.

Phase corrected rotorsynchronized pulse sequence

In single-crystal MAS NMR the signal phase is of utmost importance, because it is the observable from which the chemical shift tensor orientation is determined. A simple one-pulse excitation scheme which previously²⁵ has been used to measure single-crystal MAS NMR spectra has the disadvantage that the dead time delay needs to be compensated for by zeroth and first order phase correction of the spectra, which in turn introduces baseline rolling and a phase error which increases the further away a sideband is from the pivot-point.⁵³ A properly setup spin-echo experiment, where the delay after the π -pulse has been optimized as to minimize the need for a first-order phase correction has the advantage that the phase and amplitude of the individual spinning sidebands can be measured with higher accuracy. We therefor introduce a rotor-synchronized spin-echo experiment and doubly rotor-synchronized ramped cross-polarization followed by a spin-echo experiment which reduce phase-distortions to a tolerable level and are described in the following.

Figure 5-I shows a phase compensated 2D rotor-synchronized spin echo experiment. For rare spins (e.g. ¹³C, ¹⁵N) to achieve sensitivity, a doubly rotor-synchronized ramped based cross-polarization (CP-RAMP)⁵⁴ followed by a spin-echo pulse sequence^{55,56} is shown in Figure 5-II. In this pulse sequence the first trigger signal (t_{trig}), activated when the black-to-white contrast of the rotor meets the detector of the MAS unit, initiates the ramped based cross-polarization (CP-RAMP) sequence. After this the ¹³C/X magnetization in the xy-plane is restored to the z-direction by a $\pi/2$ pulse on X-channel which is 90° out of phase with first $\pi/2$ pulse on H-channel. When the rotor phase reaches its starting value for the next time, a second trigger signal is executed. It is then waited for a programmable t_1 period before executing the rotorsynchronized spin-echo pulse sequence.

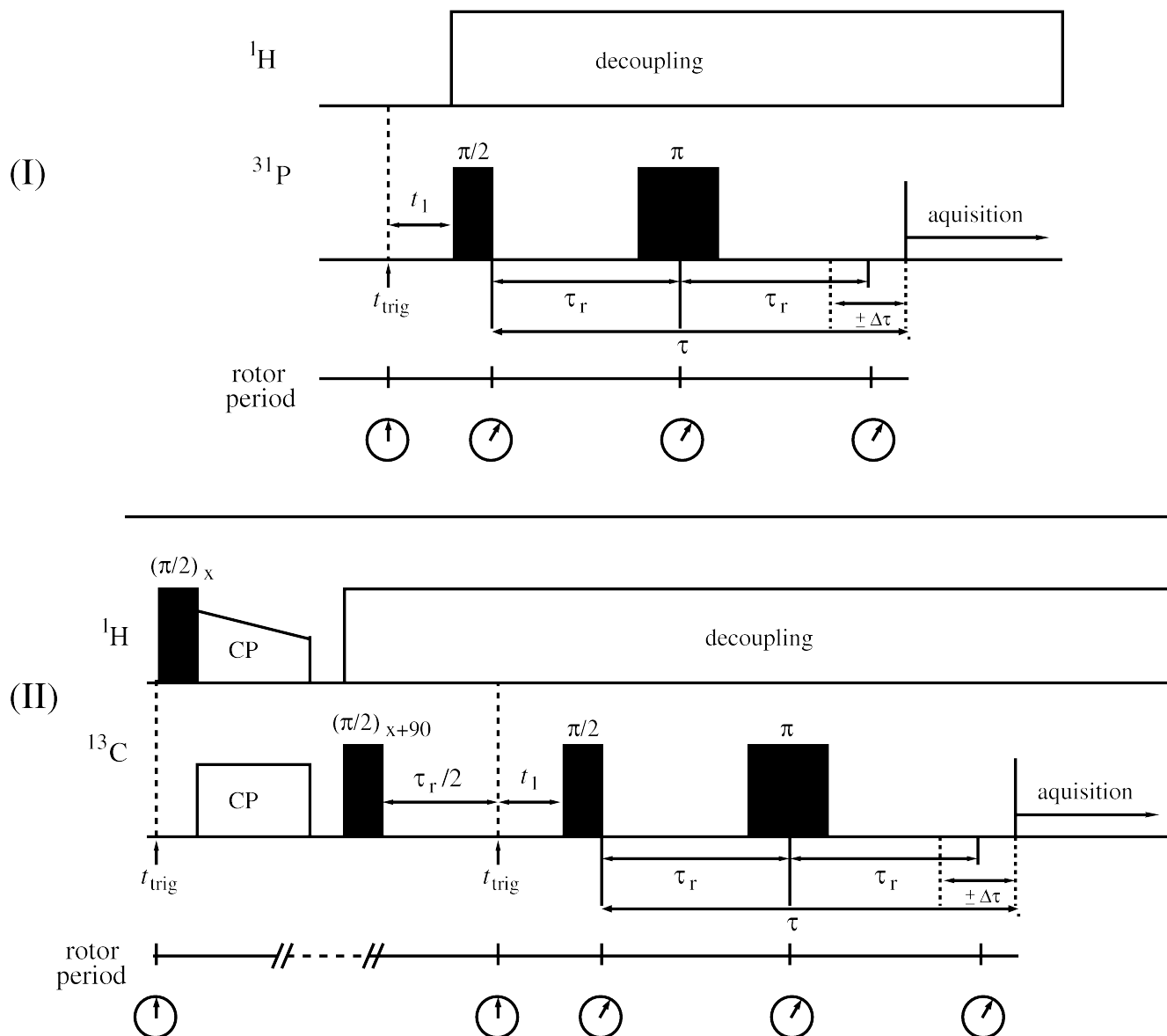


Figure 5: Rotorsynchronized two-dimensional (2D) experiments: (I) A modified 2D spin-echo pulse sequence; (II) A 2D CP-RAMP followed by a modified rotorsynchronized spin-echo pulse sequence used for single-crystal measurements; t_{trig} is the trigger signal; τ_r designates a rotor period; $\Delta\tau$ is a small delay which has to be determined once from powder measurement so that (small) first-order phase corrections become unnecessary as explained in the reference.⁵⁶

Experimental protocol

The following protocol contains the necessary steps to perform the chemical shift tensors analysis using the rotorsynchronized cross-polarization spin-echo MAS NMR of a single-crystal.

1. Determine the spectrometer constant/timing (α_0^{RL}), which is spectrometer specific and depends on the time delay between the trigger signal (t_{trig}) and rf pulse. It has to be done only once. To determine (α_0^{RL}): Do following 2-8 steps for a reference sample where the chemical shift tensor orientations are known from different sources for example from point group symmetry, static single-crystal experiments or from quantum chemical calculations.
2. Fix a single-crystal on a goniometer adapter and determine the orientation matrix by an X-ray measurement $\Rightarrow \mathbf{R}(\Omega_{CG})$.
3. Fix the goniometer adapter on the mounting equipment (Figure 4, **b**) and transfer the single-crystal into the cube (Figure 4, **e**) without changing its orientation, $\mathbf{R}(\Omega_{GW})$. Glue the single-crystal into the cube.
4. Transfer the sample cube (Figure 4, **e**) by placing the cube coordinate system parallel to the rotor coordinate system into the rotor insert (Figure 4, **j**) and place the insert into the MAS rotor (Figure 4, **k**), $\mathbf{R}(\Omega_{WR})$, so-called *parallel* orientation.
5. Obtain the phase corrected rotorsynchronized single-crystal MAS NMR spectra using pulse sequences shown in Figure 5 which does not require unwanted subsequent baseline corrections of the spectrum.
6. Similarly, obtain the rotor-synchronized single-crystal MAS NMR spectra for the second orientation by rotating the cube around \mathbf{e}_2^W by 90° in the MAS rotor insert to so-called *perpendicular* orientation.
7. Obtain the both orientations of the single-crystal in the MAS rotor system with the help of different frame transformations as shown in Figure 1, $\mathbf{R}(\Omega_{CR})$.
8. Determine the chemical shift tensor orientations from a grid search followed by a least square fitting procedure of simulated data with experimental data using the (modified³²) SIMPSON

program.^{50,51}

Experimental Section

Sample preparation

Single-crystals of ¹³C₁-labeled *L*-alanine (CAS No. 21764-56-7) and O-phosphorylethanolamine (CAS No. 1071-23-4) are grown from saturated aqueous solutions. The commercial *L*-alanine (¹³C₁, 99% enriched) and O-phosphorylethanolamine samples are purchased from the Cambridge Isotope Laboratories Inc. and Sigma, respectively. The *L*-alanine crystals are orthorhombic and belong to space-group $P2_12_12_1$ (No. 19) with four molecules per unit cell. The unit cell parameters $a=6.063 \text{ \AA}$, $b=12.261 \text{ \AA}$, $c=5.785 \text{ \AA}$ and the fractional coordinates have been determined by neutron diffraction.^{57,58} The O-phosphorylethanolamine crystals are monoclinic and belong to the spacegroup $P2_1/c$ with four molecules per unit cell. The unit cell parameters $a=9.015 \text{ \AA}$, $b=7.745 \text{ \AA}$, $c=8.788 \text{ \AA}$, and $\beta=102.51^\circ$ and fractional coordinates have been determined by neutron diffraction.⁵⁹

Solid state NMR spectroscopy

All experiments are performed on a Bruker Avance-III NMR spectrometer operating at a resonance frequency of 500.13 MHz for ¹H, 125.75 MHz for ¹³C, and 202.45 MHz for ³¹P. A commercial 4 mm triple-resonance MAS probe is used for the slow rotation of the single-crystals. The size of the crystal is chosen such that it fits into the cube (for *L*-alanine 1.2 mm × 0.8 mm × 0.9 mm and for O-phosphorylethanolamine 0.9 mm × 1.0 mm × 0.8 mm). The *L*-alanine and O-phosphorylethanolamine crystals are spun at 1.5 kHz and 4 kHz, respectively. Principal axes values of the ¹³C chemical shift tensor for the *L*-alanine were determined from a least-square fitting procedure of a simulated spectrum to an experimental slow MAS NMR spectrum as described in ref. ³². For the *L*-alanine experiment, 256 scans with repetition time delay of 3 s are accumulated per row. In total 20 different measurements are performed at changing rotor position (rotor phase γ_{CR} obtained by varying t_1) at the time of pulse irradiation by 18° between each experiment. Contact time of 3 ms is used for all experiments. Saturation pulse combs are applied prior to relaxation delays in all experiments to prepare the identical initial spin system for each transient. During all pseudo-2D experiments, we used t_1 increments and 2D

data acquisition.

Computational details

Quantum chemical calculations of absolute magnetic shielding tensors σ were performed. The experimentally determined structure of *L*-alanine from neutron diffraction at room temperature⁵⁷ served as input structure. The calculations were performed with the *Extended Embedded Ion Method* (EEIM), an embedded cluster approach in which the quantum cluster (QC, i.e. the quantum chemically treated region) is placed in an exact, self-consistent electrostatic potential, which is obtained from first principles, i.e. without empirical parameters. For details on the EEIM we refer to ref. ⁶⁰.

Two different QCs were created for EEIM calculations. The first QC included only a single alanine molecule ($[L\text{-ala}]_1$, see Figure 6 a), the second QC consisted of 15 alanine molecules ($[L\text{-ala}]_{15}$, see Figure 6 b). The pcS-2 basis set⁶¹ as stored in the Gaussian basis set library^{62,63} was used for $[L\text{-ala}]_1$, whereas a locally dense basis was used for QC $[L\text{-ala}]_{15}$, where atomic basis functions (AOs) are assigned on the basis of a spherical shell expansion around the central alanine molecule (see ⁶⁰ for details). In the innermost shell (shell range $r_1=[0,2.5[\text{ \AA}$ atomic basis functions of the pcS-2 type were used, whereas for the second shell range, $r_2=[2.5,6.0[\text{ \AA}$ the pc-1 basis⁶⁴ was used. In the third shell range, $r_3 \geq 6.0 \text{ \AA}$ the CEP-4G basis plus pseudo potentials as shipped with the GAUSSIAN 03 program were used. Further details on the cluster setup are listed in Table 1.

The GAUSSIAN 03⁶⁵ program package was used for electronic structure calculations within EEIM. The hybrid density functional mPW1PW⁶⁶ is used throughout with tight convergence criteria for the SCF. Quadrature in the DFT calculations was performed on a pruned grid of 99 radial shells and 590 angular points per shell on each atom. Atomic charges were obtained by NBO population analysis-,⁶⁷ absolute nuclear magnetic shielding tensors σ by the GIAO method.⁶⁸

Isotropic chemical shifts δ_{iso} and shift tensor eigenvalues δ_{ii} are calculated from the corresponding absolute shielding values by the conversion equation

$$\delta_{ii, calc}^{13\text{C}} = \frac{\sigma_{ii, calc}^{13\text{C}} - A}{B}, \quad i=1,2,3 \quad . \quad (25)$$

with $A = 184.599$ ppm and $B = -1.07156$, that was derived from internal calibration of the shielding tensor eigenvalues. (Figure S1 in the supplementary information shows the correlation of experimental

and calculated shielding tensor eigenvalues and the calibration line that was used to determine the parameters A and B in equation (25).) Chemical shift anisotropy parameters (CSA) are given in the *Haeberlen-Mehring-Spiess* convention^{49,69,70} i.e. in terms of the reduced anisotropy $\delta_{aniso} = \delta_{cc}^P - \delta_{iso}$ and the asymmetry $\eta = (\delta_{bb}^P - \delta_{aa}^P) / \delta_{aniso}$, where the shift tensor principal axes eigenvalues δ_{11}^P , δ_{22}^P , δ_{33}^P have been sorted according to $|\delta_{cc}^P - \delta_{iso}| \geq |\delta_{aa}^P - \delta_{iso}| \geq |\delta_{bb}^P - \delta_{iso}|$.

By default the GAUSSIAN program changes the orientation of the molecular clusters to the so-called *standard orientation* of molecular spectroscopy, which is inconvenient for the specification of the shielding tensor orientation, however. By means of a suitable rotation matrix of the kind of equation (2) we transformed the tensors to a locally defined ‘‘molecular’’ (M) Cartesian coordinate system or in terms of the crystal coordinate system (C). While we focus on the latter one for brevity in the following, the orientation in the ‘‘molecular’’ frame has some conceptual advantages and is given in the Supplemental Information.

Table 1: Setup of cluster calculations for L -alanine.

Calc.	Cluster definitions		
No	QC	Type ^a	Setup ^b
1	[L -ala] ₁ Figure 6a	EIM	mPW1PW level, pcS-2 basis for all atoms; $N_a=7$, $N_b=4$, $N_c=7$, $ N_1+N_2 =500$, $N_{rep}=1500$; $\Delta_{rms}=2.23 \times 10^{-10}$ V
2	[L -ala] ₁₅ Figure 6b	EEIM	mPW1PW level, basis in shell range $r_1 < 2.5$: pcS-2 for all atoms; range $2.5 \leq r_2 < 6.0$: pcS-1 for all atoms range $r_3 \geq 6.0$: CEP-4G basis plus pseudo potentials for all atoms; $N_a=7$, $N_b=4$, $N_c=7$, $ N_1+N_2 =600$, $N_{rep}=2300$; $\Delta_{rms}=3.88 \times 10^{-7}$ V

^a EIM=embedded ion method, EEIM=extended embedded ion method.

^b formula r_i = shortest distance to one of the atoms of the central alanine molecule, for the meaning of other symbols see ref. ⁶⁰

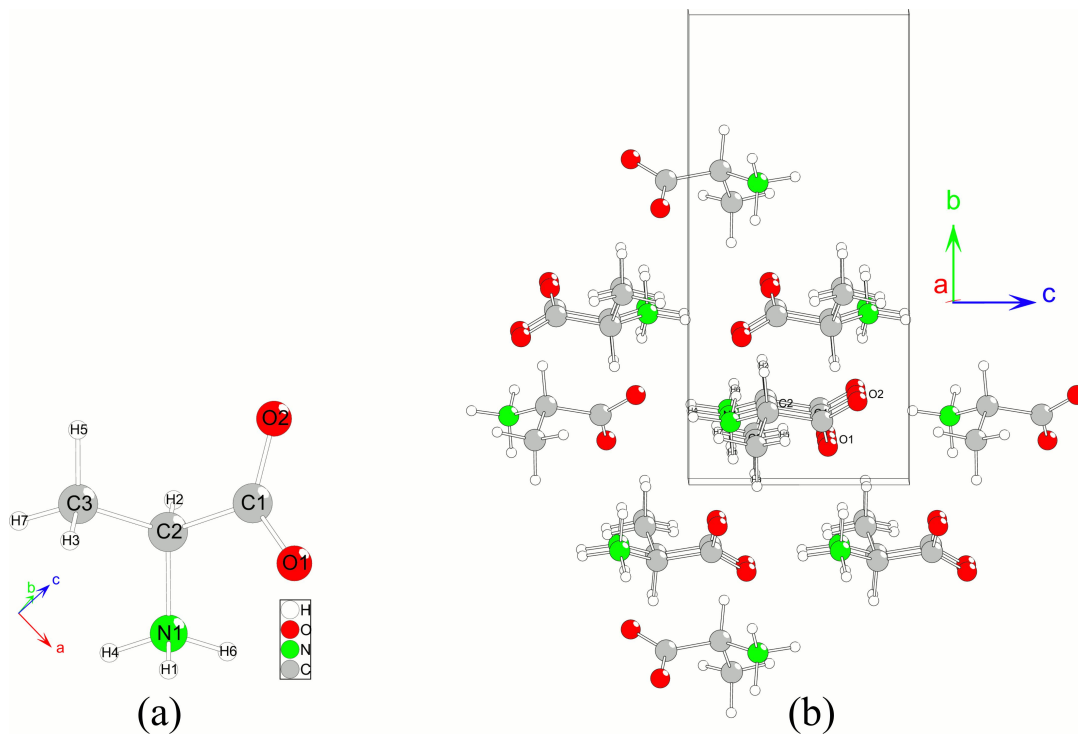


Figure 6: Quantum clusters chosen for EEIM calculations on *L*-alanine. (a): $[L\text{-ala}]_1$, (b): $[L\text{-ala}]_{15}$; all atomic sites of the central alanine unit serve as reference points for the local basis expansion; atomic site labels as in crystal structure.

Results and Discussion

In order to validate the proposed protocol and the hardware assembly for single-crystal MAS NMR experiment, single-crystals of *L*-alanine and O-phosphorylethanolamine are considered as model systems. These are well investigated compounds both with respect to their crystal structures^{57–59} and with respect to chemical shift tensors whose orientations are known from static single-crystal NMR measurements with a goniometer probe.^{2,6,21,71}

The following section starts with the discussion on the proposed protocol followed by single-crystal MAS NMR spectra for various orientations. We further discuss critical error sources which could prevent routine application of this method. Finally we discuss the derived analytical function and quantum chemical calculations.

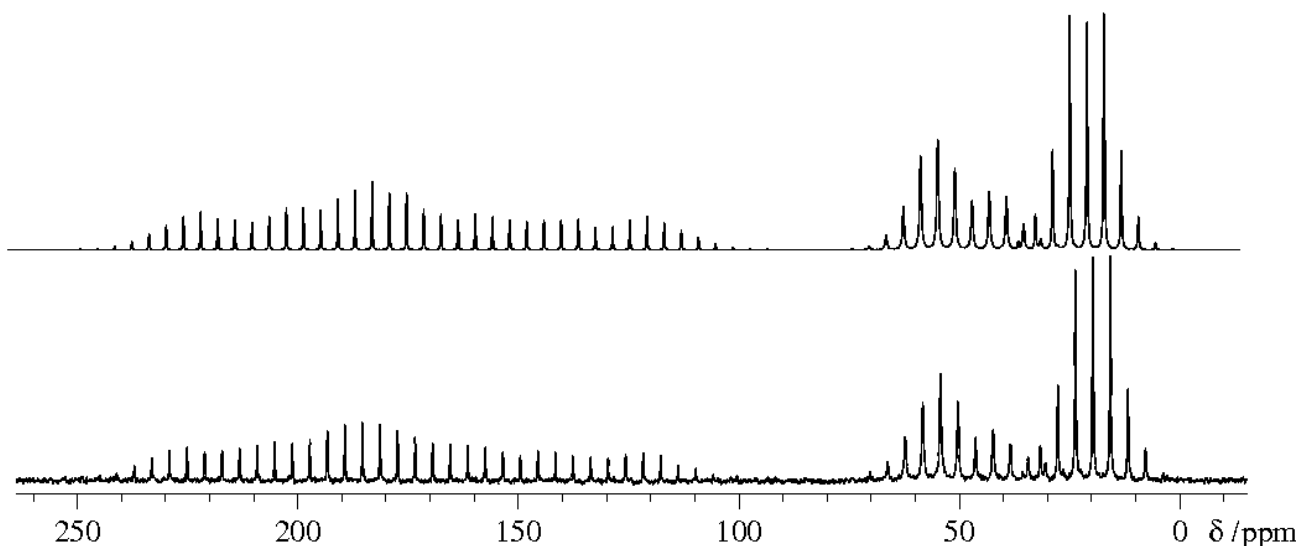


Figure 7: Slowly rotated $^{13}\text{C}\{^1\text{H}\}$ CP-MAS NMR spectrum ($\nu_{\text{MAS}} = 500\text{Hz}$) of powdered *L*-alanine (bottom) and simulated spectrum (top) using the SIMPSON program,^{50,51} the optimized CSA parameters are shown in the 2.

A ^{13}C slow MAS-NMR spectrum of a *L*-alanine powdered sample is recorded (see Figure 7) to obtain the chemical shift tensor eigenvalues and chemical shift anisotropy (CSA) parameters. The

spectrum shows three distinct signals C_A , C_B and C_C at $\delta_{iso}(C_A)=177.1$ ppm, $\delta_{iso}(C_B)=50.2$ ppm and $\delta_{iso}(C_C)=19.1$ ppm, respectively, whose assignment to the crystallographic sites has been reported in ref. 2 and is affirmed by the EEIM calculations: site C1 corresponds to signal C_A , C2 to C_B , and C3 to C_C (see also Fig. 6a). Experimental eigenvalues and CSA parameters for ^{13}C are derived from sideband patterns of the slow MAS NMR spectrum and are given together with the calculated ones in 2. Experimental and calculated values are in good agreement with root mean square deviations of $RMSD(\delta_{iso}^{exp}, \delta_{iso}^{calc})=0.7$ ppm for isotropic chemical shifts and $RMSD(\delta_{ii}^{exp}, \delta_{ii}^{calc})=1.5$ ppm for the nine shift tensor eigenvalues.

Table 2: Experimental and calculated ^{13}C chemical shift parameters of L-alanine. Calculated values use the site labeling of the crystal structure (see Figure 6), experimental signals are labeled in Figure 7. Isotropic chemical shifts are given in col. 3, CSA values in cols. 4+5. For convenience the principal axes values of the chemical shift tensor are given in col. 6-8.

Exp. and Calc.	sites	$\delta_{iso}/\text{ppm}^b$	$\delta_{aniso}/\text{ppm}^b$	η	δ_{11}/ppm^b	δ_{22}/ppm^b	δ_{33}/ppm^b	ref	
Experiment	C_A	177.09	-70.73	0.77	239.76	185.16	106.36	This work	
		175.3 ^e	-70.33 ^e	0.81 ^c	239.0 ^c	182.0 ^c	105.0 ^c	2	
		177.4 ^d							2
		176.2 ^e							2
		173.09 ^f							2
		176.8 ^g	-70.33 ^g	0.78 ^g	239±4 ^g	184±3 ^g	106±1 ^g	71	
calc. 2 (Figure 6 b)	C_1	176.4	-72.8	0.745	239.8	185.6	103.6	This work	
(calc. 1 (Figure 6 a)	C_1	177.1	-73.1	0.766	241.7	185.7	104.0)	This work	
Experiment	C_B	50.22	-18.96	0.59	65.36	54.05	31.27	This work	
		50.7 ^d							2
		50.5 ^e							2
		49.44 ^f							2
		50.9 ^g	-19.66 ^g	0.35 ^g	63±1 ^g	56±1 ^g	30±3 ^g	71	
calc. 2 (Figure 6 b),	C_2	51.1	-20.8	0.502	66.8	56.3	30.3	This work	
(calc. 1 (Figure 6 a)	C_2	52.1	-22.7	0.444	68.4	58.4	29.4)	This work	
Experiment	C_C	19.73	11.49	0.96	31.23	19.54	8.42	This work	
		20.0 ^d							2
		19.5 ^e							2

		15.97 ^f						2
		19.8 ^g	-12.0 ^g	1.0 ^g	31±2 ^g	19±2 ^g	7±2 ^g	71
calc. 2 (Figure 6 b)	C ₃	19.7	-12.4	0.806	30.8	20.9	7.3	This work
(calc. 1 (Figure 6 a)	C ₃	16.5	-21.2	0.584	33.2	20.9	-4.7)	This work

^a calculated values for the central alanine molecule in the QC are given.

^b chemical shifts calculated from absolute magnetic shieldings according to equation (25).

^c experimental chemical shifts values from static measurement (ref 2)

^d experimental chemical shifts values from MAS (powder sample) measurement (ref 2)

^e experimental chemical shifts values from single-crystal measurement (ref 2)

^f experimental chemical shifts values from solution pH=0.7 (ref 2)

^g experimental chemical shifts values from MAS (powder sample) measurement (ref ⁷²)

Discussion of the protocol

To perform an accurate chemical shift tensors analysis, it is important to determine the precise orientation of the single-crystal in the rotor system by an independent X-ray measurement. A precise determination of the Euler angles between the crystal axis and the rotor system (Ω_{CR}) is required (see Figure 1). The problem of simulating single-crystal MAS pattern is solved only after the calculation of a set of these three Euler angles.

In order to find out Ω_{CR} , following transformations are carried out. The Euler angles between the crystal coordinate system (C) and the diffractometer coordinate system (D) (Ω_{CD}) are obtained via an X-ray measurement. The orientation of the single-crystal relative to the goniometer coordinate system (G) is necessary and calculated by a rotation matrix, $\mathbf{R}(\Omega_{CG})$, using $\mathbf{R}(\Omega_{CG})=\mathbf{R}(\Omega_{DG})\cdot\mathbf{R}(\Omega_{CD})$ transformation, where, $\mathbf{R}(\Omega_{DG})$ is the rotation matrix from (D) to (G) coordinate system. As explained previously (theory section), these two frames are not identical and in our case differ by $\varphi=0.56^\circ\pm 0.36^\circ$. This could be one of the important sources of error if neglected. Note that this mapping is diffractometer dependent and for other diffractometers φ is very likely different. Hence, an accurate determination of $\mathbf{R}(\Omega_{CG})$ is possible (Experimental protocol, step-2).

Similarly, a set of Euler angles between the goniometer coordinate system (G) and the cube coordinate system (W) is calculated. Here we considered the following mapping: $\mathbf{e}_1^G\|\mathbf{e}_3^W$, $\mathbf{e}_2^G\|\mathbf{e}_1^W$ and

Avadhut *et al.* (2017).

$\mathbf{e}_3^G \parallel \mathbf{e}_2^W$. Hence, the rotation matrix from C to W is calculated using $\mathbf{R}(\Omega_{CW}) = \mathbf{R}(\Omega_{GW}) \cdot \mathbf{R}(\Omega_{CG})$ transformation (Experimental protocol, step-3).

Further we obtain the L -alanine single-crystal MAS NMR spectra with the "default" and "non-default" cube orientation so called *parallel* and *perpendicular* orientation, respectively (Experimental protocol, step-4 to step-6), using a doubly rotor-synchronized ramped cross polarization followed by spin-echo experiment (Figure 5-II).

Now it is possible to calculate the required set of Euler angles between the C and R coordinate system, (Ω_{CR}) , using $\mathbf{R}(\Omega_{CR}) = \mathbf{R}(\Omega_{WR}) \cdot \mathbf{R}(\Omega_{CW})$ transformation (experimental protocol, step-7). In the case of L -alanine, for *parallel* orientation we obtained: $\alpha_{CR} = 275.37^\circ$, $\beta_{CR} = 14.29^\circ$, $\gamma_{CR} = 22.1^\circ$, and *perpendicular* orientation: $\alpha_{CR} = 118.108^\circ$, $\beta_{CR} = 79.3^\circ$, $\gamma_{CR} = 174.525^\circ$ are calculated. Error analysis of the present NMR data shows that the Euler angles describing the orientation of the crystal coordinate system relative to the rotor coordinate system are determined with an accuracy of $\pm 0.5^\circ$.

It is also necessary to determine the orientation of the single-crystal relative to the trigger marking of the rotor. Further we note explicitly, that the correct angle γ_{CR} in real experiment also depends on 1) the time delay between the trigger signal and the rf pulse which is depending on the spectrometer and 2) the probe construction, i.e., the MAS detector position of the glass fiber. However this timing problem can be eliminated by calibration of spectrometer constant/timing α_0^{RL} . This has to be done only once for the spectrometer using any single-crystal with precisely determined chemical shift tensor (Experimental protocol, step-1). A single-crystal of O-phosphorylethanolamine is used to calibrate spectrometer constant. In our case, the spectrometer constant is calculated as $273.04^\circ \pm 0.05^\circ$.

Discussion of single-crystal spectra

The rotorsynchronized MAS patterns of the L -alanine single-crystal are plotted in Figure 8 and Figure 9 with the *parallel* and the *perpendicular* orientations, respectively. In both figures the experimental spectrum is shown on the top and the simulations are plotted underneath using the calculated Euler angles, Ω_{CR} (Experimental protocol, step-7), and the spectrometer constant α_0^{RL} (Experimental protocol, step-1). These plots provide an overall visual comparison of the changes of the spectra

Avadhut *et al.* (2017).

depending on the rotor position which is indicated by the angle γ_{CR} .

Clearly, the two spectra sets are distinctly different as is to be expected because in the first case, the cube axes are parallel to the rotor axes whereas in the second case, it is perpendicular when rotating around the \mathbf{e}_2^W axis by 90° . The spectral extension of the spinning sidebands are comparable due to fact that that angle between rotor axis and the external magnetic field \mathbf{B}_0 is $\approx 54.74^\circ$. After a full rotor period identical MAS spectra are obtained in the both cases.

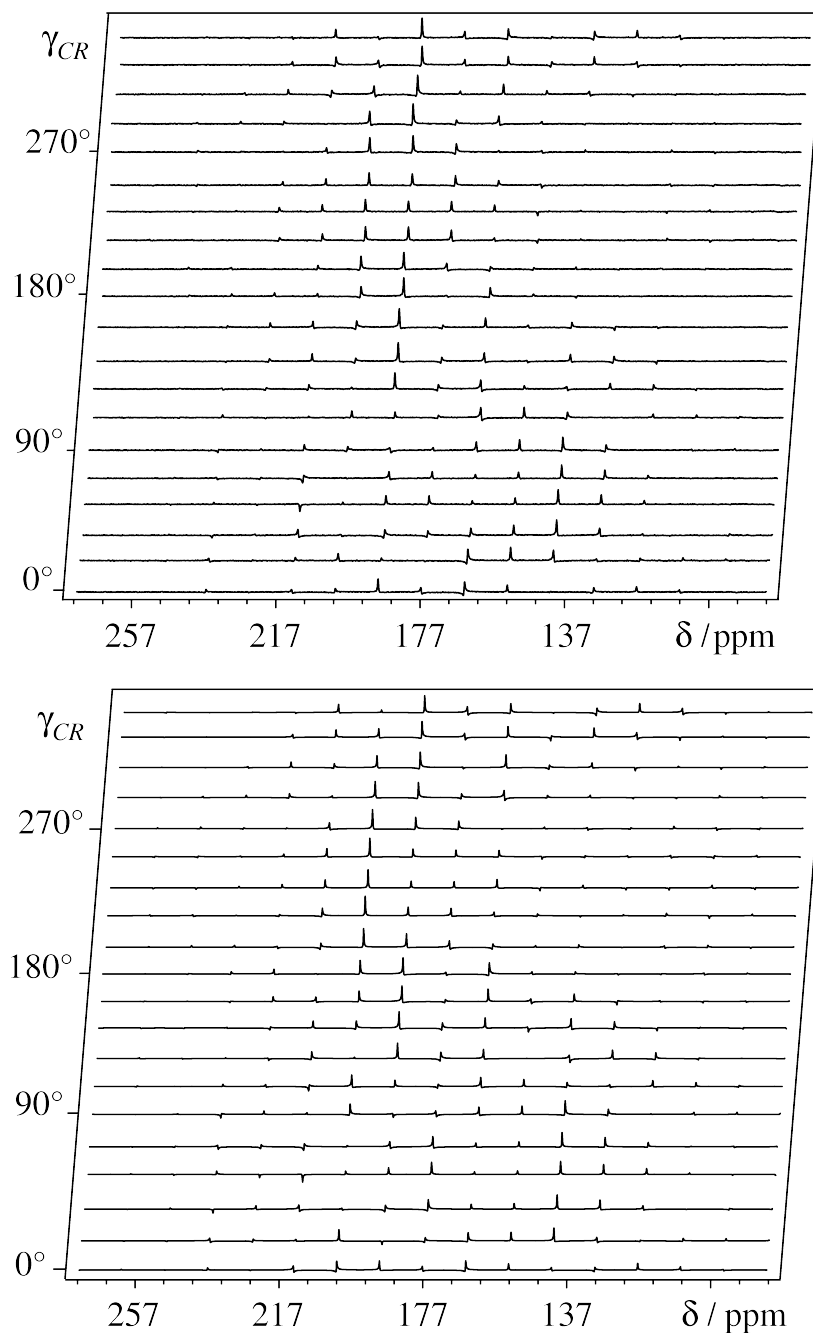


Figure 8: Comparison of (top) experimental rotorsynchronized $^{13}\text{C}\{^1\text{H}\}$ CP-MAS NMR spectra of *L*-alanine with (bottom) simulations for cube axes parallel to the rotor axes; the simulation parameters are: $\delta_{11}=239.7$ ppm $\delta_{22}=185.1$ ppm , $\delta_{33}=106.3$ ppm , $\alpha_{PC}=348.87^\circ$, $\beta_{PC}=94.99^\circ$, $\gamma_{PC}=127.92^\circ$, $\alpha_{CR}=275.37^\circ$, $\beta_{CR}=14.29^\circ$, $\gamma_{CR}=22.1^\circ$, and $\alpha_0^{RL}=273.04^\circ$.

In this test case of *L*-alanine, the orientation of the $^{13}\text{C}_1$ chemical shift tensor is determined with the

Avadhut *et al.* (2017).

help of exact initial orientation of the single-crystal when the rf pulse is applied. The problem of simulating both the orientation patterns is simplified since only the rotor angle γ_{CR} is found for which the simulation of the MAS pattern taken for the whole rotor cycle, matches the experimental spectrum (Experimental protocol, step-8). The result is shown in the bottom spectrum of the Figure 8 and the Figure 9. It is now possible to follow the various changes of the line shapes as functions of the rotor angle and there is clearly convincing coincidence between the simulated data and the experimental data.

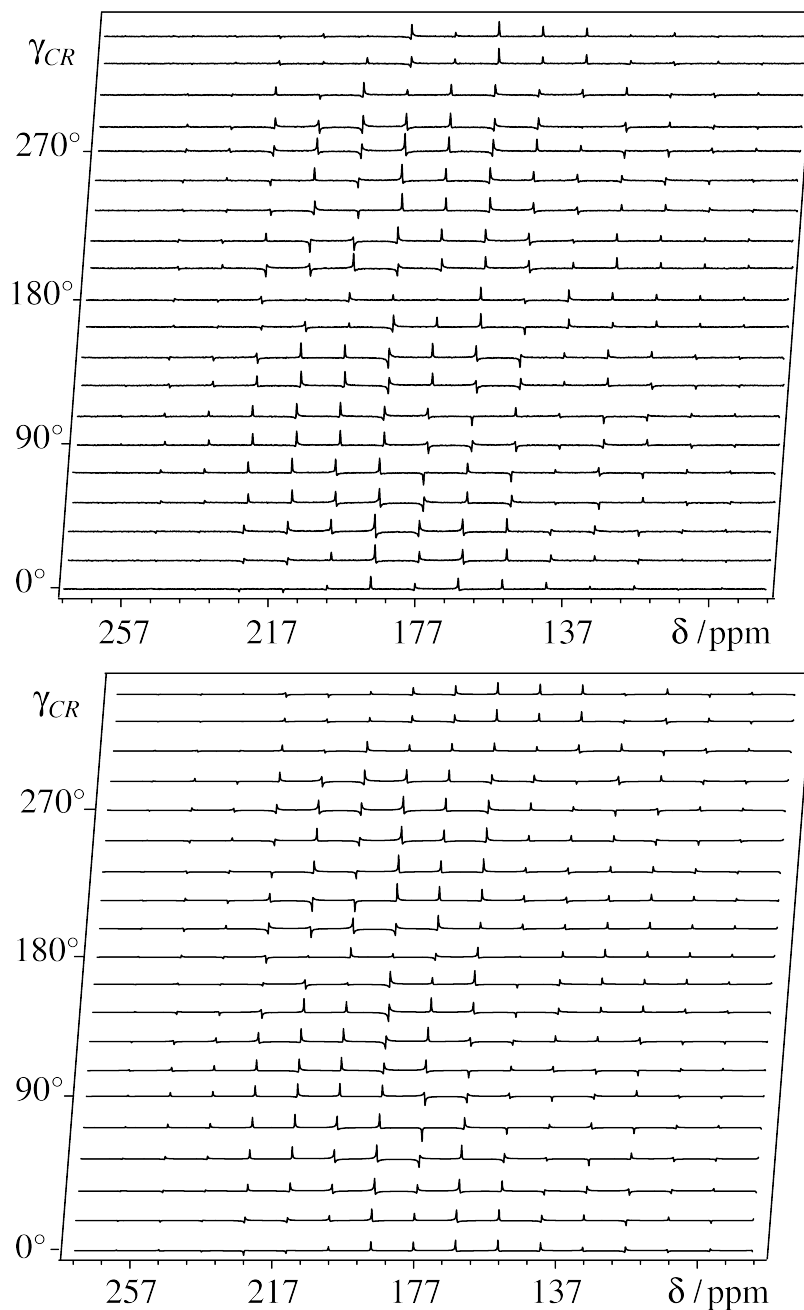


Figure 9: Comparison of (top) experimental rotorsynchronized $^{13}\text{C}\{^1\text{H}\}$ CP-MAS NMR spectra of L-alanine with (bottom) simulations for cube axes perpendicular to the rotor axes; the simulation parameters are: $\delta_{11}=239.7$ ppm $\delta_{22}=185.1$ ppm, $\delta_{33}=106.3$ ppm, $\alpha_{PC}=348.87^\circ$, $\beta_{PC}=94.99^\circ$, $\gamma_{PC}=127.92^\circ$, $\alpha_{CR}=118.1^\circ$, $\beta_{CR}=79.3^\circ$, $\gamma_{CR}=174.52^\circ$, and $\alpha_0^{RL}=273.04^\circ$.

Error analysis

There are minor deviations between the simulated and the experimental pattern possibly due to the following error sources. One of the major source of error is instabilities in the MAS frequency. Typically, for $1.5\text{ kHz} \pm 1\text{ Hz}$ sample spinning frequency, the error is about $\pm 0.24^\circ$. The rotation of the single-crystal inside the rotor does not cause any instabilities, possibly because the plastic insert adds a significant amount of mass which is homogeneously distributed in the rotor. As described in the hardware section, the cube was chosen such that it fits into the rotor insert but it does not mean that it is tightly fixed by the rotor insert wall. In our case, the cube has an angular deviation of 0.024° inside the rotor insert along the rotor axis. Hence it might well be the case that the crystallographic axis can be tilted slightly with respect to the rotor axis during measurements which causes the error in the Euler angle set $\mathbf{R}(\Omega_{CR})$ (see Figure 1 and protocol step-7). Another source of error can be from X-ray diffractometer which can determine the crystal to laboratory orientation within 0.01° accuracy which affects/influences the starting Euler angle set $\mathbf{R}(\Omega_{CG})$ (see Figure 1 and protocol step-2). Moreover, a further source of error could be caused by fixing the single-crystal from the goniometer into the cylindrical void of the cube and hence the set of Euler angle $\mathbf{R}(\Omega_{GW})$ (see Figure 1 and protocol step-3). However, in our case this possible source of error is negated by holding the mounting tool vertically. Some minor errors can occur while fixing the standard goniometer adapter on the homemade single-crystal mounting tool (Figure 4) which is neglected in this work.

The simulations have shown, that the chemical shift tensors and their orientations in the crystal coordinate system can be determined with an accuracy about $\pm 1^\circ$. The angular deviations of the tensor orientations from the single-crystal MAS and the traditional static single-crystal NMR², and the single-crystal MAS and the quantum chemical calculations are given in the supplemental information for the three tensor eigenvectors $\mathbf{e}_i^P(C_1)(i=1,2,3)$.

Numerical Validation

In order to estimate an accuracy for the orientation determination, we have evaluated the complete set of rotorsynchronized spectra over a full rotor period using the derived analytical function. For the parallel and the perpendicular orientations, the line intensities and the phases of the dispersive spinning

Avadhut *et al.* (2017).

sidebands are plotted in the Figure 10. The calculated intensities and the phases of complete 2D patterns for both the orientations are seen to agree closely with experimentally measured values.

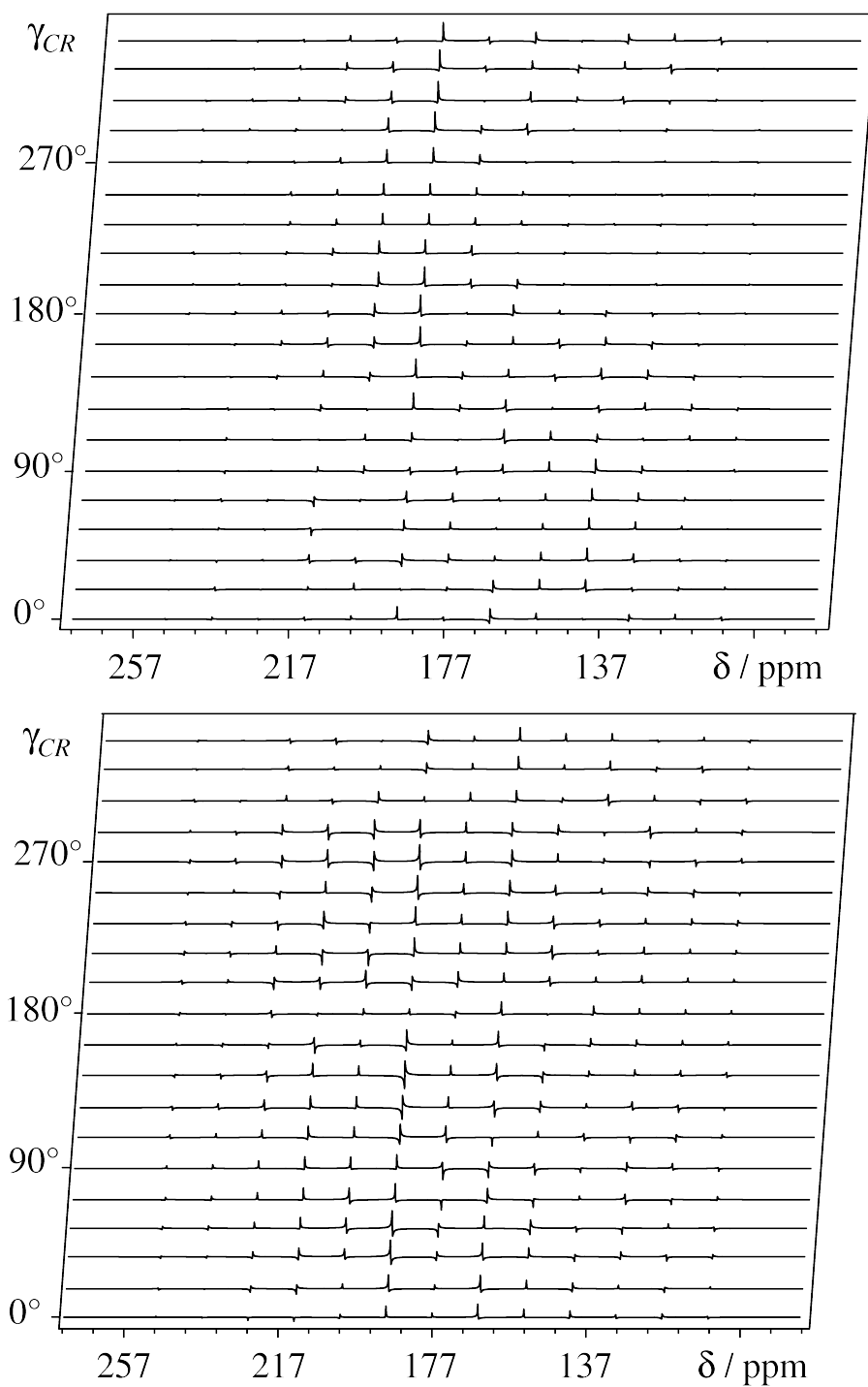


Figure 10: Spectra obtained using the derived analytical function for (top) parallel and (bottom) perpendicular orientations; the theoretical parameters are same as simulation parameters (see Figure 8 and Figure 9).

To compare the simulated spectra and the spectra obtained from the derived analytical function with the experimental data in more detail few selected slices taken from Figure 9 and Figure 10 (bottom), respectively, are shown in Figure 11. The simulated spectra and the spectra from the analytical function are slightly shifted towards left (b) and right (c) with respect to the experimental spectra (a), such that all line shapes can be compared more easily. Additionally, the sum projection from all rotor positions obtained by experiment is compared with the simulated sum projection by using calculated α_{CR} , β_{CR} , and γ_{CR} for both the orientations (shown in the supplementary information) which shows all spinning sidebands are absorptive and positive.

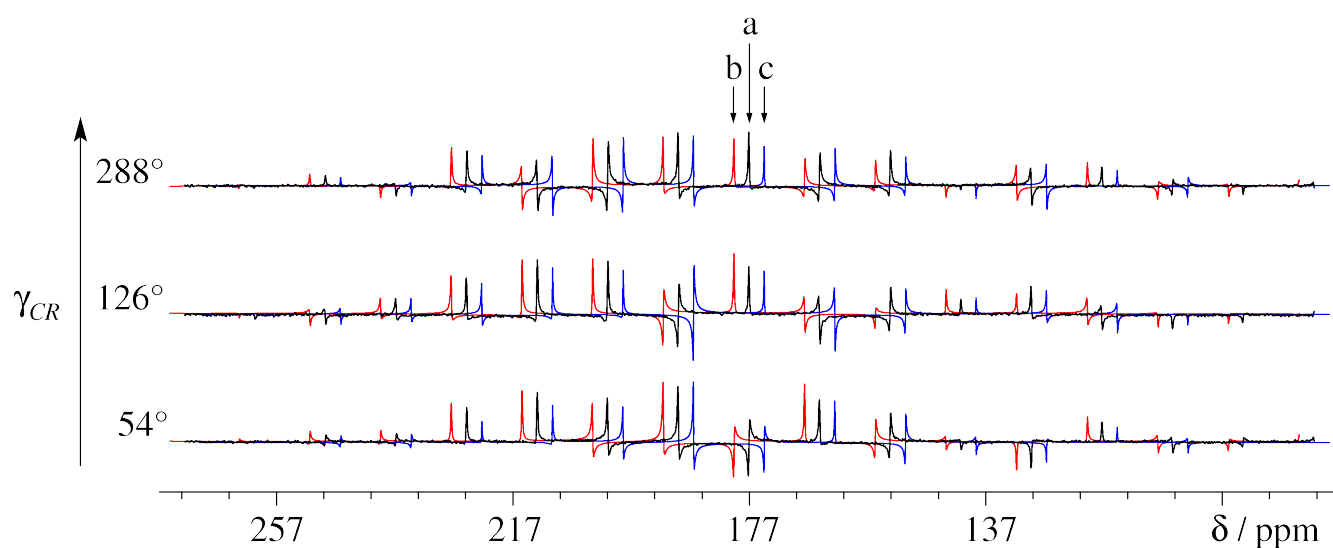


Figure 11: Comparison of three slices for *perpendicular* orientation of the rotorsynchronized MAS NMR spectra (a) with the corresponding simulations (b) taken from Figure 9 and spectra obtained using the derived analytical function (c) taken from Figure 10 (bottom); the simulated spectra and the spectra obtained by the analytical function are slightly shifted towards the left and the right to the experimental spectra, respectively.

The chemical shift tensor orientations of the $^{13}\text{C}_1$ with respect to the crystal coordinate system obtained by the MAS and the static NMR is shown in Figure 12. Additionally, tensor direction cosines of the $^{13}\text{C}_1$ from the MAS and the static are compared in reference 3. Hence, we can anticipate that with the presented approach, the determination of the chemical tensors including their orientations can be made as precise as with the traditional static single-crystal NMR.

Orientation relative to the crystal axis system

The orientation of the chemical shift tensors with respect to the crystal axes a , b , c is shown in Figure 12 and is given in terms of direction cosines in Table 3. The tensors are shown in ellipsoid representation⁷³ with eigenvectors of principal axis system relative to the crystal axis system. Table 3 contains also the Euler angles for the rotation matrices $\mathbf{R}(\alpha_{PC}(\text{C1}), \beta_{PC}(\text{C1}), \gamma_{PC}(\text{C1}))$ which transform the P - of site C1 to the C coordinate system as well as the Euler angles for the rotation matrix $\mathbf{R}(\alpha_{CP}(\text{C1}), \beta_{CP}(\text{C1}), \gamma_{CP}(\text{C1}))$ for the back-transformation from the C - to the P - coordinate system. The chemical shift tensors of symmetry-related, crystallographically identical sites (e.g. C1^a and C1^b) have different orientations relative to the crystal axis system.

The values obtained by single-crystal MAS compare well with those from Naito *et al.*² and with calculated ones obtained with the EEIM method (see Figure 12 and T

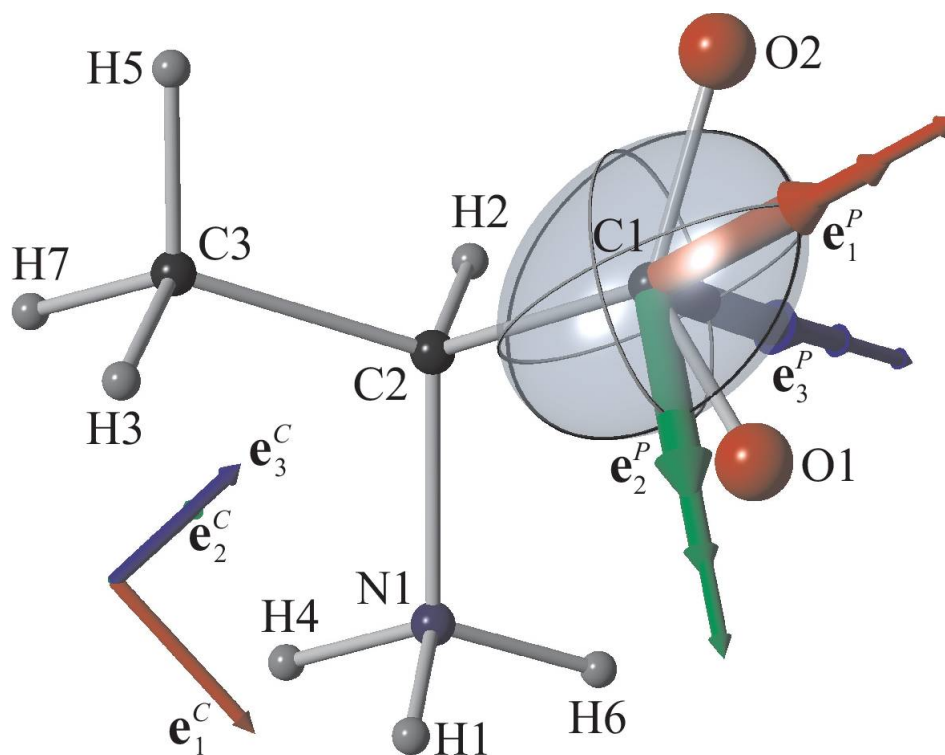


Figure 12: ^{13}C chemical shift tensors orientation of $^{13}\text{C}_1$ -labeled *L*-alanine in comparison to the molecular frame and the crystal axis system $\{\mathbf{e}_1^C, \mathbf{e}_2^C, \mathbf{e}_3^C\}$ from MAS (*thick*), static (*intermediate*), and EEIM (*thin*); all C-atoms were created by symmetry operation (x, y, z); tensors are shown in ellipsoid representation⁶⁰ with eigenvectors \mathbf{e}_1^P (red), \mathbf{e}_2^P (green), and \mathbf{e}_3^P (blue) relative to the crystal axis system (\mathbf{e}_1^C (red), \mathbf{e}_2^C (green), and \mathbf{e}_3^C (blue)); atomic site labels as in crystal structure.

Table 3: Direction cosines of chemical shift tensors of $^{13}\text{C}_1$ -labeled *L*-alanine to the respective crystal coordinate system

Site	Method	Eigenvectors	\mathbf{e}_1^C	\mathbf{e}_2^C	\mathbf{e}_3^C	Euler Angles ^a		Euler Angles ^a	
C1 ^b (COO-) (carboxy)	MAS	\mathbf{e}_1^P	0.203786	-0.052516	0.977605	α_{PC}	348.869	α_{CP}	52.079
	Static ^c	\mathbf{e}_1^P	0.2005	-0.0719	0.9771	α_{PC}	348.669	α_{CP}	52.963
	EEIM	\mathbf{e}_1^P	0.190040	-0.071526	0.979167	α_{PC}	348.785	α_{CP}	52.676
	MAS	\mathbf{e}_2^P	0.763899	-0.616009	-0.192330	β_{PC}	94.899	β_{CP}	94.899
	Static	\mathbf{e}_2^P	0.7737	-0.6025	-0.2029	β_{PC}	93.7154	β_{CP}	93.7154
	EEIM	\mathbf{e}_2^P	0.773018	-0.603945	-0.194147	β_{PC}	93.4101	β_{CP}	93.4101
	MAS	\mathbf{e}_3^P	0.612314	0.785986	-0.085416	γ_{PC}	127.919	γ_{CP}	191.129
	Static	\mathbf{e}_3^P	0.6011	0.7966	-0.0648	γ_{PC}	127.038	γ_{CP}	191.331
	EEIM	\mathbf{e}_3^P	0.605250	0.793810	-0.059483	γ_{PC}	127.324	γ_{CP}	191.215
C1 ^d (carboxy)	MAS	\mathbf{e}_1^P	-0.203786	0.052516	0.977605	α_{PC}	348.869	α_{CP}	232.079
	EEIM	\mathbf{e}_1^P	-0.190040	0.071526	0.979167	α_{PC}	348.785	α_{CP}	232.676
	MAS	\mathbf{e}_2^P	-0.763899	0.616009	-0.192330	β_{PC}	94.899	β_{CP}	94.899
	EEIM	\mathbf{e}_2^P	-0.773018	0.603945	-0.194147	β_{PC}	93.4101	β_{CP}	93.4101
	MAS	\mathbf{e}_3^P	-0.612314	-0.785986	-0.085416	γ_{PC}	307.919	γ_{CP}	191.129
C1 ^e (carboxy)	EEIM	\mathbf{e}_3^P	-0.605250	-0.793810	-0.059483	γ_{PC}	307.324	γ_{CP}	191.215
	MAS	\mathbf{e}_1^P	-0.203786	-0.052516	-0.977605	α_{PC}	168.869	α_{CP}	127.920
	EEIM	\mathbf{e}_1^P	-0.190040	-0.071526	-0.979167	α_{PC}	168.785	α_{CP}	127.324
	MAS	\mathbf{e}_2^P	-0.763899	-0.616009	0.192330	β_{PC}	85.100	β_{CP}	85.100
	EEIM	\mathbf{e}_2^P	-0.773018	-0.603945	0.194147	β_{PC}	86.5899	β_{CP}	86.590
C1 ^f (carboxy)	MAS	\mathbf{e}_3^P	-0.612314	0.785986	0.085416	γ_{PC}	52.080	γ_{CP}	11.129
	EEIM	\mathbf{e}_3^P	-0.605250	0.793810	0.059483	γ_{PC}	52.6759	γ_{CP}	11.215
	MAS	\mathbf{e}_1^P	0.203786	0.052516	-0.977605	α_{PC}	168.869	α_{CP}	307.920
	EEIM	\mathbf{e}_1^P	0.190040	0.071526	-0.979167	α_{PC}	168.785	α_{CP}	307.324
	MAS	\mathbf{e}_2^P	0.763899	0.616009	0.192330	β_{PC}	85.100	β_{CP}	85.100
C1 ^f (carboxy)	EEIM	\mathbf{e}_2^P	0.773018	0.603945	0.194147	β_{PC}	86.5899	β_{CP}	86.590
	MAS	\mathbf{e}_3^P	0.612314	-0.785986	0.085416	γ_{PC}	232.080	γ_{CP}	11.129

Avadhut *et al.* (2017).

EEIM	\mathbf{e}_3^P	0.605250	-0.793810	0.059483	γ_{PC} 232.676	γ_{CP} 11.215
------	------------------	----------	-----------	----------	-----------------------	----------------------

^a All angles in degree

^b Atoms created by symmetry operation x, y, z

^c Experimental direction cosines from Naito *et al.*². formula $\mathbf{e}_2^P(C1)$ and formula $\mathbf{e}_3^P(C1)$ inverted (corresponds to a rotation around formula $\mathbf{e}_1^P(C1)$ by 180°).

^d Atoms created by symmetry operation $-x+0.5, -y, z+0.5$

^e Atoms created by symmetry operation $-x, y+0.5, -z+0.5$

^f Atoms created by symmetry operation $x+0.5, -y+0.5, -z$

Conclusions

For the first time, we have shown that rotor-synchronized single-crystal MAS-NMR spectra can give access to full tensor information (eigenvalues and eigenvectors), even if the tensor has an arbitrary orientation with respect to the crystal frame. We have given a full implementation in theory as well as in hardware and have suggested a protocol, which can be used to obtain accurate chemical shift tensor orientations with respect to any of the typically used frames, of which the crystal or the molecular frame are frequently used.

A cost-effective homemade single-crystal mounting tool provides high accuracy for mounting and remounting a single-crystal in various orientations inside the magic angle spinning rotor with the stability of MAS frequency. The proposed hardware assembly is a mandatory, essential, and primary requirement to use this method as a routine tool and may be transferred to different rotor types as well as rotor sizes. The specialized homemade rotor insert design achieves stable spinning frequencies up to 15 kHz. A thorough/detailed experimental protocol based on phase corrected, rotor-synchronized pulse sequences leads to full chemical shift tensor information as precise as with typical static single-crystal NMR experiments. An analytical function is derived to calculate the intensities and phases of the dispersive line shape of the spinning sidebands and yields shift tensor orientations that agree closely (deviations below $\pm 1^\circ$ in Euler angles) with calculated values or those determined by static experiments. The derived analytical function may lead to a software development for deconvolution since it allows fast calculation of single-crystal MAS spectra. As an example, the chemical shift tensor orientations of $^{13}\text{C}_1$ -labeled *L*-alanine in the crystal coordinate system are determined and supported by quantum chemical EEIM calculations.

The potential advantages of this method are low cost, large resolution enhancement, use of standard MAS probes, and considerable time saving compared to the traditional static single-crystal NMR. Further, this method offers better spectral resolution in case of small single-crystals due to suppression of dipole-dipole couplings by magic angle spinning. A foreseeable application is to obtain chemical shift tensor orientations in partially oriented materials. Also, this method can be extended to all other rank 2 interaction tensors detectable by NMR. An extension to quadrupolar tensors/electric field gradients by the piggyback/microcoil design was already done in the mean time²⁷, although for a simple case, where the quadrupolar tensor orientation coincides with the symmetry axes of the crystal.

Our method can be used as a routine/standard tool to determine the tensors in arbitrary orientations with respect to the crystal frame. Furthermore, it could become useful to study motion and dynamics in crystals, for example ion dynamics, which would add a spatial dimension to the NMR analysis which is lacking in many of the standard NMR techniques. Finally, tensor orientation data may help to determine the space-group in difficult cases, that are not solvable by X-ray diffraction alone. When the accuracy shielding tensor orientations is of primary interest, the selective excitation of similarly oriented crystallites may only comprise a tiny subset, which has a effectively smaller sample volume than the our used single crystals.

Acknowledgment

We gratefully acknowledge financial support through the Emmy-Noether program of the DFG (SCHM1570-2). We also grateful to Prof. Dr. W. Schnick for the possibility to use the facilities at the chair of inorganic solid-state chemistry. We thank the Leibniz-Rechenzentrum for computational resources. We acknowledge to Prof. Dr. O. M. Oeckler and Prof. Dr. U. Müller for useful discussions. We also thank C. Minke and T. Miller for technical support.

Supporting Information Available

References

- (1) MacKenzie, K. J. D.; Smith, M. E. *Multinuclear Solid-State Nuclear Magnetic Resonance of Inorganic Materials*; Pergamon, 2002; Vol. 6.
- (2) Naito, A.; Ganapathy, S.; Akasaka, K.; McDowell, C. A. *J. Chem. Phys.* **1981**, *74* (6), 3190.
- (3) Lauterbur, P. *Phys. Rev. Lett.* **1958**, *1* (9), 343.
- (4) Janes, N.; Ganapathy, S.; Oldfield, E. *J. Magn. Reson.* **1983**, *54* (1), 111.
- (5) Sherwood, M. H.; Alderman, D. W.; Grant, D. M. *Journal of Magnetic Resonance (1969)* **1989**, *84* (3), 466.
- (6) Vinding, M. S.; Kessler, T. O.; Vosegaard, T. *Journal of Magnetic Resonance* **2016**, *269*, 120.
- (7) Haberkorn, R. A.; Stark, R. E.; Van Willigen, H.; Griffin, R. G. *J. Am. Chem. Soc.* **1981**, *103* (10), 2534.
- (8) Griffin, R. G.; Ellett, J. D.; Mehring, M.; Bullitt, J. G.; Waugh, J. S. *J. Chem. Phys.* **1972**, *57* (5), 2147.

- (9) Van Calsteren, M.; Birnbaum, G. I.; Smith, I. C. P. *J. Chem. Phys.* **1987**, *86* (10), 5405.
- (10) Kohler, S. J.; Ellett, J. D.; Klein, M. P. *J. Chem. Phys.* **1976**, *65*, 2922.
- (11) Kohler, S. J.; Ellett, J. D.; Klein, M. P. *J. Chem. Phys.* **1976**, *64* (11), 4451.
- (12) Herzfeld, J.; Griffin, R. G.; Haberkorn, R. A. *Biochem.* **1978**, *17* (14), 2711.
- (13) Spiess, H. W.; Haas, H.; Hartmann, H. *J. Chem. Phys.* **1969**, *50* (7), 3057.
- (14) Lauterbur, P. C.; Burke, J. J. *J. Chem. Phys.* **1965**, *42* (1), 439.
- (15) Pausak, S.; Pines, A.; Waugh, J. S. *J. Chem. Phys.* **1973**, *59* (2), 591.
- (16) Pines, A.; Chang, J. J.; Griffin, R. G. *J. Chem. Phys.* **1974**, *61* (3), 1021.
- (17) Pausak, S.; Tegenfeldt, J.; Waugh, J. S. *J. Chem. Phys.* **1974**, *61* (4), 1338.
- (18) Honkonen, R. S.; Doty, F. D.; Ellis, P. D. *J. Am. Chem. Soc.* **1983**, *105* (13), 4163.
- (19) Vosegaard, T.; Langer, V.; Daugaard, P.; Hald, E.; Bildsoe, H. *Rev. Sci. Instrum.* **1996**, *67* (6), 2130.
- (20) Griffin, R. G.; Powers, L.; Pershan, P. S. *Biochem.* **1978**, *17* (14), 2718.
- (21) Kohler, S. J.; Klein, M. P. *Biochem.* **1976**, *15* (5), 967.
- (22) Kohler, S. J.; Klein, M. P. *Biochem.* **1977**, *16* (3), 519.
- (23) Murray, D. K.; Harrison, J. C.; Wallace, W. E. *J. Colloid Interface Sci.* **2005**, *288* (1), 166.
- (24) Pell, A. J.; Pintacuda, G.; Emsley, L. *The Journal of Chemical Physics* **2011**, *135* (14), 144201.
- (25) Kunath-Fandrei, G. H.; Kelbaskas, L.; Döring, D.; Rager, H.; Jäger, C. *Phys. Chem. Miner.* **1998**, *26* (1), 55.
- (26) Klymachyov, A. N.; Dalal, N. S. *Zeitschrift für Physik B Condensed Matter* **1997**, *104* (4), 651.
- (27) Vasa, S. K.; Ernst, R. H. van E.; Janssen, J. W. G.; Kentgens, A. P. M. *Phys. Chem. Chem. Phys.* **2010**, *12*, 4813.
- (28) Kentgens, A. P. M.; Bart, J.; van Bentum, P. J. M.; Brinkmann, A.; van Eck, E. R. H.; Gardeniers, J. G. E.; Janssen, J. W. G.; Knijn, P.; Vasa, S.; Verkuijlen, M. H. W. *J. Chem. Phys.* **2008**, *128* (5), 052202.
- (29) Kentgens, A. P. M.; Bart, J.; van Bentum, P. J. M.; Brinkmann, A.; van Eck, E. R. H.; Gardeniers, J. G. E.; Janssen, J. W. G.; Knijn, P.; Vasa, S.; Verkuijlen, M. H. W. *The Journal of Chemical Physics* **2008**, *128* (5), 052202.
- (30) Harbison, O. S.; Spiess, H. W. *Chem. Phys. Lett.* **1986**, *124* (2), 128.
- (31) Levitt, M. H. *J. Magn. Reson.* **1989**, *82* (2), 427.
- (32) Avadhut, Y. Quantitative solid state nuclear magnetic resonance methods for inorganic materials. Text.PhDThesis, Ludwig-Maximilians-Universität München, 2012.
- (33) Pell, A. J.; Pintacuda, G. *Progress in Nuclear Magnetic Resonance Spectroscopy* **2015**, *84–85*, 33.
- (34) Pell, A. J.; Clement, R. J.; Grey, C. P.; Emsley, L.; Pintacuda, G. *J. Chem. Phys.* **2013**, *138* (11), 114201.

- (35) Antzutkin, O. N. *Prog. Nucl. Magn. Reson. Spectrosc.* **1999**, 35 (3), 203.
- (36) Maricq, M. M.; Waugh, J. S. *J. Chem. Phys.* **1979**, 70 (7), 3300.
- (37) Herzfeld, J.; Berger, A. E. *J. Chem. Phys.* **1980**, 73 (12), 6021.
- (38) Rose, M. E. *Elementary Theory of Angular Momentum*; Dover Publications Inc., 1995.
- (39) Schmidt-Rohr, K.; Spiess, H. W. *Multidimensional Solid-State NMR and Polymers*; Academic Press, 1994.
- (40) Levitt, M. H. *Spin Dynamics: Basics of Nuclear Magnetic Resonance*, 2nd ed.; John Wiley & Sons, 2008.
- (41) Olejniczak, E. T.; Vega, S.; Griffin, R. G. *J. Chem. Phys.* **1984**, 81 (11), 4804.
- (42) Antzutkin, O. N.; Shekar, S. C.; Levitt, M. H. *J. Magn. Reson. A* **1995**, 115 (1), 7.
- (43) Mehring, M. *High-Resolution NMR in solids, in NMR Basic Principles and Progress*; Springer, Berlin, 1976; Vol. 11.
- (44) Kreyszig, E. *Advanced Engineering Mathematics*, 10th ed.; Wiley, 2011.
- (45) Arfken, G. B.; Weber, H. J. *Mathematical Methods for Physicists, Fourth Edition*, 4th ed.; Academic Press, 1995.
- (46) Abramowitz, M.; Stegun, I. A. *Handbook of mathematical functions with formulas, graphs, and mathematical tables*; Courier Dover Publications, 1964.
- (47) Hahn, T. *International tables for crystallography, Volume A*, 5th ed.; Springer Dordrecht: The Netherland, 2005; Vol. A.
- (48) Weil, J. A.; Buch, T.; Clapp, J. E. In *Advances in Magnetic and Optical Resonance*; John S. Waugh, Ed.; Academic Press, 1973; Vol. Volume 6, pp 183–257.
- (49) Mehring, M. *Principles of High Resolution NMR in Solids*, 2nd ed.; Springer-Verlag Berlin, 1983; Vol. 87.
- (50) Bak, M.; Rasmussen, J. T.; Nielsen, N. C. *J. Magn. Reson.* **2000**, 147 (2), 296.
- (51) Vosegaard, T.; Malmendal, A.; Nielsen, N. C. *Monatshefte für Chemie* **2002**, 133 (12), 1555.
- (52) Hansen, M. R.; Vosegaard, T.; Jakobsen, H. J.; Skibsted, J. *J. Phys. Chem. A* **2004**, 108 (4), 586.
- (53) Slichter, C. P. *Principles of Magnetic Resonance*, 3rd ed.; Springer Berlin Heidelberg, 1992.
- (54) Metz, G.; Wu, X. L.; Smith, S. O. *J. Magn. Reson. A* **1994**, 110 (2), 219.
- (55) Hahn, E. *Phys. Rev.* **1950**, 80 (4), 580.
- (56) Avadhut, Y. S.; Schneider, D.; Schmedt auf der Günne, J. *J. Magn. Reson.* **2009**, 201 (1), 1.
- (57) Wilson, C. C.; Myles, D.; Ghosh, M.; Johnson, L. N.; Wang, W. *New J. Chem.* **2005**, 29 (10), 1318.
- (58) Lehmann, M. S.; Koetzle, T. F.; Hamilton, W. C. *J. Am. Chem. Soc.* **1972**, 94 (8), 2657.
- (59) Weber, H.-P.; McMullan, R. K.; Swaminathan, S.; Craven, B. M. *Acta Cryst. B* **1984**, 40 (5), 506.
- (60) Weber, J.; Schmedt auf der Günne, J. *Phys. Chem. Chem. Phys.* **2009**, 12 (3), 583.
- (61) Jensen, F. *J. Chem. Theory Comput.* **2008**, 4 (5), 719.
- (62) Feller, D. *J. Comp. Chem.* **1996**, 17 (13), 1571.

Avadhut *et al.* (2017).

- (63) Schuchardt, K. L.; Didier, B. T.; Elsethagen, T.; Sun, L.; Gurumoorthi, V.; Chase, J.; Li, J.; Windus, T. L. *J. Chem. Inf. Model.* **2007**, *47* (3), 1045.
- (64) Jensen, F. *J. Chem. Phys.* **2001**, *115* (20), 9113.
- (65) Frisch, M. J. *GAUSSIAN 03 program, Revision D.01*; 2004.
- (66) Adamo, C.; Barone, V. *J. Chem. Phys.* **1998**, *108* (2), 664.
- (67) Glendering, E. D.; Badenhop, J. K.; Reed, A. E.; Carpenter, J. E.; Bohmann, J. A.; Morales, C. M.; Weinhold, F. *Theoretical Chemistry Institute, University of Wisconsin, Madison, WI* No. 2001.
- (68) Wolinski, K.; Hinton, J. F.; Pulay, P. *J. Am. Chem. Soc.* **1990**, *112* (23), 8251.
- (69) Haeberlen, U. *High resolution NMR in solids: Advances in Magnetic Resonance, Suppl. 1*; Academic Press: New York, 1976.
- (70) Spiess, H. W. *NMR Basic Principles and Progress*, 2nd ed.; Springer, Berlin, 1978; Vol. 15.
- (71) Kohler, S. J.; Klein, M. P. *J. Am. Chem. Soc.* **1977**, *99* (25), 8290.
- (72) Ye, C.; Fu, R.; Hu, J.; Hou, L.; Ding, S. *Magn. Reson. Chem.* **1993**, *31* (8), 699.
- (73) Radeglia, R. *Solid State Nucl. Magn. Reson.* **1995**, *4* (5), 317.